ACS MATERIALS Au
AN OPEN ACCESS JOURNAL OF THE AMERICAN CHEMICAL SOCIETY

pubs.acs.org/materialsau
Review

Spin Effects in Optimizing Electrochemical Applications

Published as part of ACS Materials Au special issue "2024 Rising Stars".

Cunyuan Gao and Bin Cai*

Cite This: *ACS Mater. Au* 2025, 5, 253−267
Read Online
ACCESS | Metrics & More | Article Recommendations

ABSTRACT: Efficient electrocatalyst development is crucial for addressing global energy challenges, and recent advances have highlighted the significant role of electron spin—a fundamental property of electrons—in influencing catalytic processes. Regulating the spin states of active sites has emerged as a powerful strategy to enhance catalytic performance. In response to growing interest in spin-induced electrocatalysis, this review offers a comprehensive examination of the impact of spin states on electrocatalytic activity. We explore various strategies for modulating spin states, review state-of-the-art techniques for spin state characterization, and elucidate the mechanisms by which spin effects enhance catalytic efficiency. Additionally, we discuss future research directions, emphasizing the potential of spin regulation to drive innovation in electrocatalyst design and application. This review aims to provide a foundational understanding of spin effects in electrocatalysis, guiding future efforts in the rational design of high-performance catalysts.

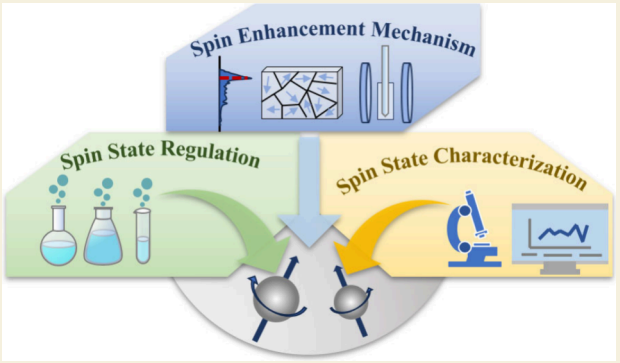

KEYWORDS: *Spin, Electronic structure, d-band theory, Electrocatalysis, Magnetization, Spin selection, Oxygen evolution, Activity descriptor*

1. INTRODUCTION

The growing consumption of fossil fuels and consequent environmental degradation have driven the advancement of sustainable energy conversion technologies, such as water electrolysis,[1−3] fuel cells,[3,4] metal-air batteries,[5−7] and the electrochemical reduction of carbon dioxide[8,9] and nitrogen.[10,11] High-performance electrocatalysts are crucial for the industrial application of these technologies. In recent years, substantial efforts have been devoted to understanding the intrinsic reaction mechanisms and structure-performance relationships in electrocatalysis, and various principles and descriptors have been proposed to guide the construction of efficient electrocatalysts.[12−17] Among them, the Sabatier principle proposes that the interaction between the catalyst surface and the reactants should optimally balance—not too strong nor too weak.[18] Additionally, the *d*-band center theory proposed by Nørskov et al. reveals the relationship between their electronic structure and intrinsic activity.[14,19,20] However, further refinement of the *d*-band center theory is still necessary to analyze electronic structures at a more granular level.

Recently, spin—an intrinsic property of electrons—has emerged as a promising degree of freedom for modulating the electronic structure of catalyst surfaces, offering new opportunities for catalyst design.[21−23] Recent studies have demonstrated that altering the spin state of the active centers in electrocatalysts can modulate the adsorption strength of reaction intermediates at the catalytic sites, thereby enhancing catalytic activity.[24] Furthermore, the spin configuration of the catalysts can influence charge transport during electrochemical reactions and then accelerate reaction kinetics.[25] Despite these advancements, there is still a lack of a systematic review on the spin regulation in electrocatalysts, the characterization of spin states, and the impact of spin effects on catalyst performance.

Given the significant impact of spin on the electronic structure and catalytic performance of active sites, there remains a critical need for a systematic exploration of spin regulation in electrocatalysis. This review aims to address this gap by first outlining key strategies for modulating spin states during catalyst preparation. We then examine advanced techniques for characterizing spin states and analyze the mechanisms through which spin effects enhance catalytic activity. Finally, we offer perspectives on emerging trends and future research directions

Received: August 28, 2024
Revised: November 22, 2024
Accepted: November 25, 2024
Published: November 30, 2024

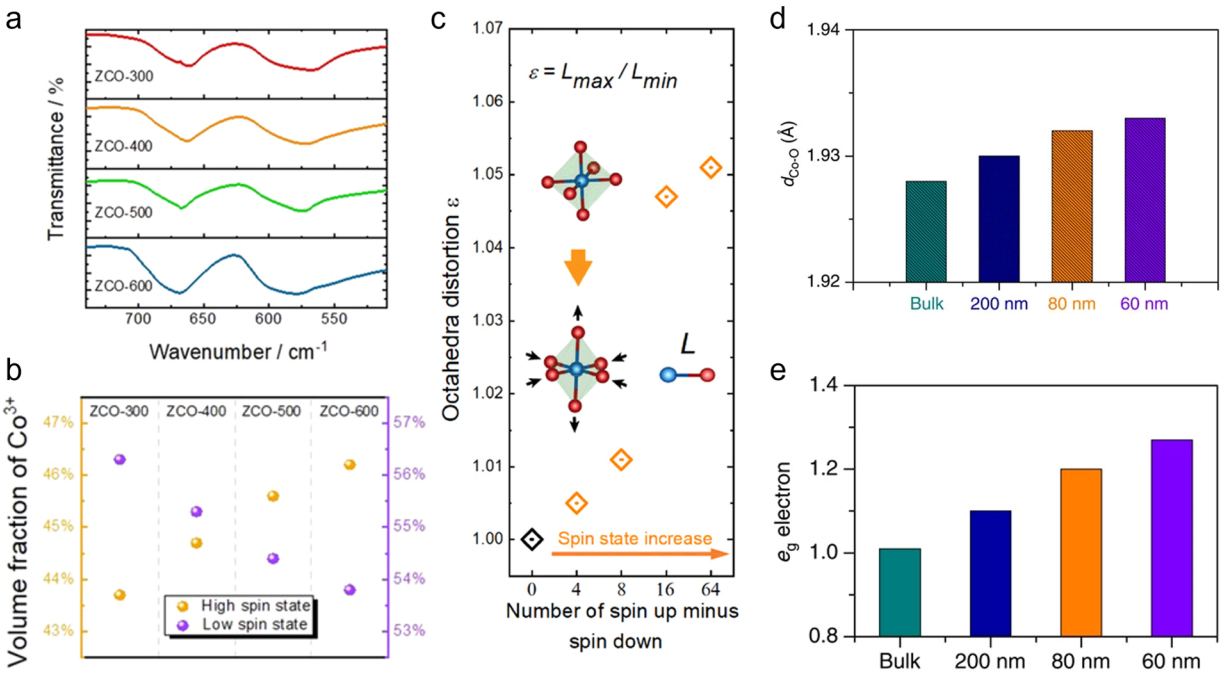

Figure 1. **a** FTIR spectra of the as-prepared spinel $ZnCo_2O_4$. **b** The volume fraction of high state and low state Co^{3+} in the spinel $ZnCo_2O_4$. **c** The octahedra distortion during spin state increase in $ZnCo_2O_4$. Reprinted with permission from Reference [38]. Copyright 2021 Wiley-VCH. **d** Co−O bond length for $LaCoO_3$ with different diameters. **e** The e_g electron of $LaCoO_3$ with different diameters. Reprinted with permission under a CC-BY 4.0 license from Reference [26]. Copyright 2016 Springer Nature.

in spin-regulated electrocatalysis, with the goal of inspiring new approaches to the rational design of high-performance catalysts.

2. STRATEGIES FOR THE REGULATION OF SPIN STATES

The electronic structure of active sites directly influences the adsorption behavior of catalytic intermediates, thereby affecting catalytic activity.[19] Controlling the spin states of active metals has emerged as a promising strategy for precisely tuning their electronic structures. Recently, various strategies have been developed for controlling the spin states of metal-based active sites, including size modulation,[26−28] defective engineering,[29,30] doping,[31−33] magnetic field synergy[34−36] and metal-carrier interactions.[33,37] These strategies offer effective avenues for exploring mechanisms underlying spin-promoted catalysis.

2.1. Tuning Size

Adjusting the size of the catalyst can induce lattice distortions, thereby altering the spin state of the active center.[27,28] The size of $ZnCo_2O_4$ spinel oxide nanoparticles increases with the calcination temperature.[38] The Fourier Transform Infrared (FTIR) spectroscopy (Figure 1a) and Superconducting Quantum Design (SQUID) measurements (Figure 1b) show that higher calcination temperatures intensify lattice distortions, resulting in an increase in high spin state Co^{3+}. Density functional theory (DFT) calculations confirm that an increase in unpaired spins within $ZnCo_2O_4$ leads to more pronounced lattice distortions in the octahedral units (Figure 1c). Similarly, $LaCoO_3$ perovskite oxides with different particle sizes can be synthesized by varying the annealing temperature.[26] This size variation causes changes in Co−O bond lengths, resulting in spin state transitions of Co^{3+}. In bulk $LaCoO_3$, the e_g filling ratio is approximately 1.0, with high-spin and low-spin Co^{3+} states each constituting 50% (Figure 1d). However, when the particle size is reduced to 80 nm, Co^{3+} undergoes spin state transitions, increasing the proportion of high-spin states and raising the e_g orbital electron occupancy to 1.2 (Figure 1e). This size effect facilitates controllable regulation of the active sites spin state, offering a reliable method for subsequent performance optimization.

2.2. Defect Engineering

The coordination structure of the active center significantly impacts their spin states. The introduction of defects can alter the coordination environment of the active sites, thereby inducing spin state transitions.[29,30] The Co^{3+} usually exhibits a low-spin configuration in CoOOH. However, by introducing unsaturated coordinated Co atoms, a high spin CoOOH structure was successfully synthesized.[39] The high spin state Co^{3+} configuration is verified via SQUID (Figure 2**a-b**), X-ray absorption spectroscopy (XAS) (Figure 2**c-d**), and electron paramagnetic resonance (EPR) (Figure 2e), exhibiting ferromagnetism behavior with unpaired electrons and 3*d* and 4*p* orbitals splitting. This high spin CoOOH demonstrated remarkable oxygen evolution reaction (OER) activity, with an overpotential of 226 mV at 10 mA cm^{-2} (Figure 2f). In $PrBaCo_2O_6$, varying oxygen vacancy concentrations lead to an alternating structure of pyramid-shaped $Co^{3+}O_5$ and octahedral $Co^{3+}O_6$ in the PrO layer, inducing a transition of Co^{3+} from a high spin to a low spin.[40]

2.3. Heteroatom Doping

Doping heteroatoms near active sites can induce distortions in the coordination structure, breaking the local symmetry of the active center and triggering spin state transitions.[31−33] For instance, introducing Mn around Fe sites effectively stimulates the spin state transition of Fe^{3+} (Figure 3a).[31] The Mn atoms disrupt the local Fe−N symmetry, resulting in the delocalization of Fe^{3+} electrons and inducing a spin state transition from low spin ($t_{2g}^5e_g^0$) to Intermediate spin ($t_{2g}^4e_g^1$) (Figure 3**b-c**). Beyond transition metals, the spin state of carbon materials can

https://doi.org/10.1021/acsmaterialsau.4c00092
ACS Mater. Au 2025, 5, 253−267

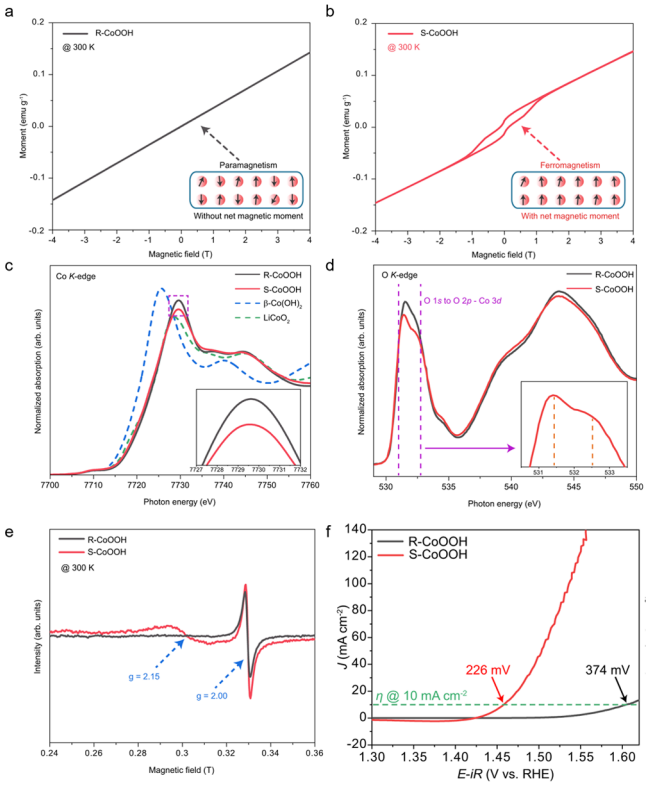

Figure 2. **a** Magnetic hysteresis loop of R-CoOOH. **b** Magnetic hysteresis loop of S-CoOOH. **c** Co K-edge XAS spectra. **d** O K-edge XAS spectra. **e** EPR spectra of R-CoOOH and S-CoOOH. **f** Cyclic voltammetry (CV) curves of R-CoOOH and S-CoOOH. Reprinted with permission under a CC-BY 4.0 license from Reference [39]. Copyright 2024 Springer Nature.

also be regulated through atom doping. Yang et al. investigated the nitrogen reduction reaction (NRR) catalytic activity of carbon-based materials doped with O, S, Se, and Te atoms using experimental and theoretical methods (Figure 3d).[41] Their calculations revealed that heteroatom doping promotes charge accumulation, enhancing N_2 adsorption on carbon atoms. Spin-resolved density pictures demonstrated that heteroatom doping generates noticeable spin moments on nonmagnetic carbon atoms (Figure 3e). This spin polarization effect facilitates the first protonation to form the *NNH chemical step in NRR, thereby improving catalytic activity (Figure 3f).

2.4. Magnetic Field Synergy

The spin state of the active metal site is intrinsically linked to the overall magnetism of the material. Consequently, the application of a magnetic field can play a crucial role in spin regulation. When an external magnetic field is applied, the magnetic moments of the material align with the direction of the field at a macroscopic level, resulting in spin polarization. It should be noted that this phenomenon is restricted to ferromagnetic materials. Xu et al. demonstrated that $Co_{3-x}Fe_xO_4$ oxides[42] and NiFe films[43] can be used to regulate spin-polarized electrons and enhance OER efficiency under a magnetic field (Figure 4**a-c**). Furthermore, the Co and Mn ions in a nonprecious metal–organic framework, characterized by thermally differentiated superlattice structures, undergo magnetothermal stimulation to induce spin changes in the active Co^{3+} center (Figure 4d).[44] The presence of a thermal insulation layer mitigates lattice distortion within the structure, while the magnetic field prompts spin reconstruction of the metal ions. After treatment, the active center Co^{3+} transitions from a high-spin to low-spin, thereby modulating the OER activity (Figure 4e).

2.5. Metal–Carrier Interaction

The spin states of metal centers can be modulated by the structural diversity of different supports. Single-atom catalysts are more strongly influenced by their supports compared to nanocrystal catalysts.[33,37] Fe single atoms anchored on ultrathin TiO_2 nanoribbons via an adsorption oxidation strategy exhibit a shift in the *d*-band center of Fe 3*d* to a higher energy level, while

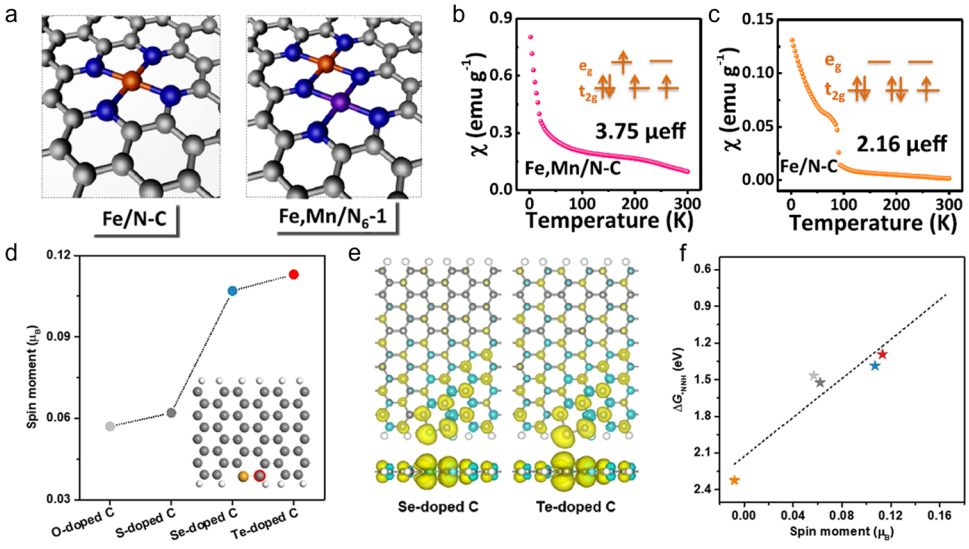

Figure 3. **a** The optimized structure of Fe/N–C and Fe,Mn/N–C. **b** Magnetic susceptibility of Fe,Mn/N–C (Intermediate spin Fe^{3+}). **c** Magnetic susceptibility of Fe/N–C (low spin Fe^{3+}). Reprinted with permission under a CC-BY 4.0 license from Reference [31]. Copyright 2021 Springer Nature. **d** Spin moment of carbon atom of different doping materials, the red part of the model diagram represents the corresponding carbon atom. **e** Top view and side view of the spin-resolved density map of Se-doped C on the left, top view and side view of the isosurface of the spin-resolved density pictures of Te-doped C on the right. **f** The correlation between the spin moment and ΔG_{*NNH}. Reprinted with permission from Reference [41]. Copyright 2020 Wiley-VCH.

https://doi.org/10.1021/acsmaterialsau.4c00092
ACS Mater. Au 2025, 5, 253–267

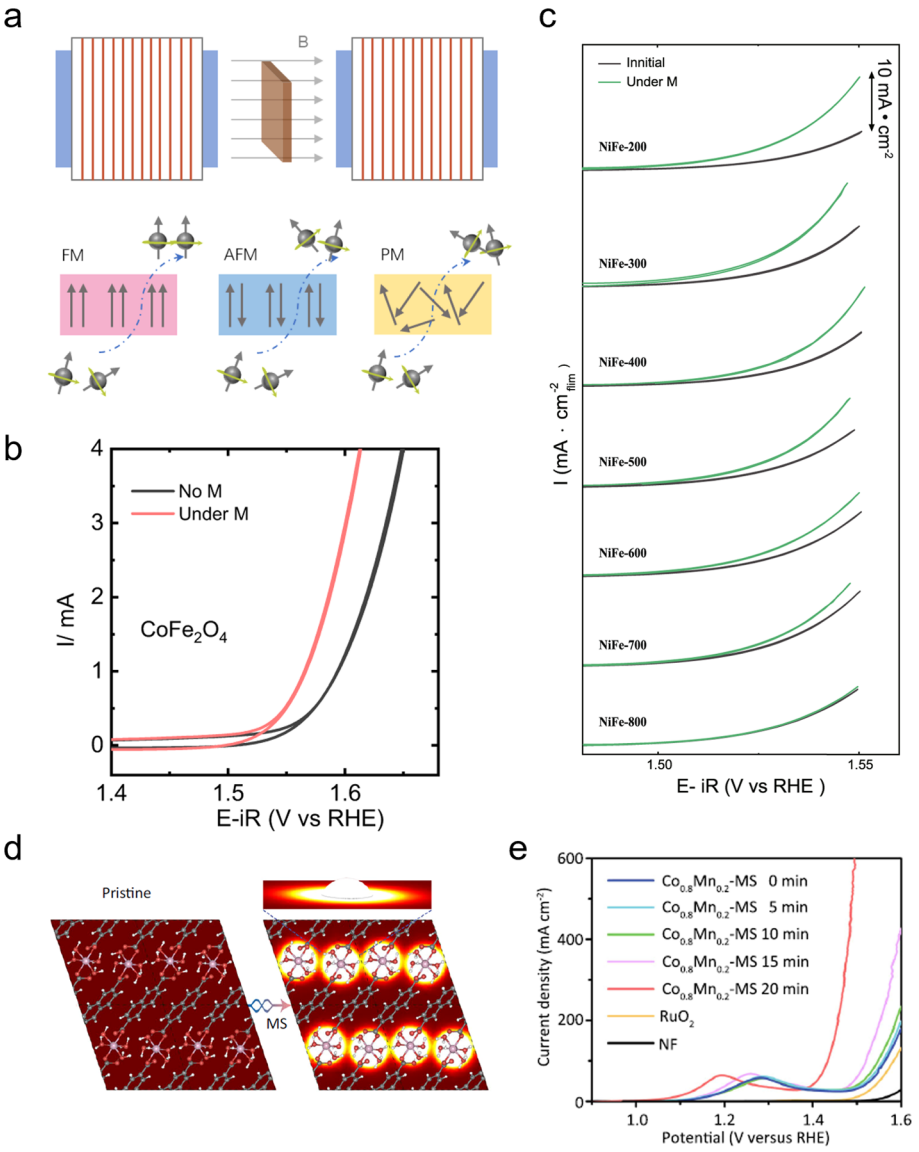

Figure 4. a Schematic diagram of the generation of the polarized electron under a constant magnetic field. **b** CV curves of $CoFe_2O_4$ with and without magnetic field. Reprinted with permission under a CC-BY 4.0 license from Reference [42]. Copyright 2021 Springer Nature. **c** CV curves of NiFe thin films with different thicknesses with and without magnetic field. Reprinted with permission under a CC-BY 4.0 license from Reference [43]. Copyright 2023 Springer Nature. **d** Schematic diagram of active sites of magnetic effect precision heating catalyst. **e** CV curves of the $Co_{0.8}Mn_{0.2}$-MOF with different times of MS. Reprinted with permission under a CC-BY 4.0 license from Reference [44]. Copyright 2021 Springer Nature.

the d-band center of Ti 3*d* shifts to a lower level.[37] This strong metal−support interaction between Fe and TiO_2 leads to a transition of Fe^{3+} from a high-spin to a low-spin state. Similarly, the spin configuration of Co single atoms can be regulated through metal−support interactions.[45] For instance, when Co single atoms are loaded onto TaS_2 monolayers, the spin state of Co is modulated by adjusting the loading amount of Co.

3. SPIN STATE TRANSITION CHARACTERIZATION

Inducing spin state changes is a powerful strategy for achieving precise control over electronic structures. Advanced characterization techniques are crucial for identifying and analyzing these spin state transitions. Significant efforts have been made to develop these techniques, including vibrating sample magnetometry (VSM), EPR, Mössbauer spectroscopy, XAS, and electron energy loss spectroscopy (EELS). The following sections detail the analytical methods employed by these characterization techniques.

3.1. Vibrating Sample Magnetometer

Spin state transitions can be identified by changes in the material's magnetic properties. The VSM is a highly sensitive magnetic measurement tool based on the principle of electrical induction.[46,47] It can measure the magnetic moment as a function of temperature (known as M-T), allowing for the calculation of the magnetic moment of the material, which is closely related to the number of unpaired electrons.[48] At relatively high temperatures (T > 150 K), thermal fluctuations dominate magnetic ionic interactions, resulting in a magnetically disordered paramagnetic state. In this region, the magnetic susceptibility (χ = M/H) calculated from the magnetization intensity follows the Curie−Weiss law. The calculated Curie constant can be used to derive the effective magnetic moment of each ion using the formula ($\mu_{eff} = \sqrt{8C}\mu_B$, where μ_B is Bohr

https://doi.org/10.1021/acsmaterialsau.4c00092
ACS Mater. Au 2025, 5, 253−267

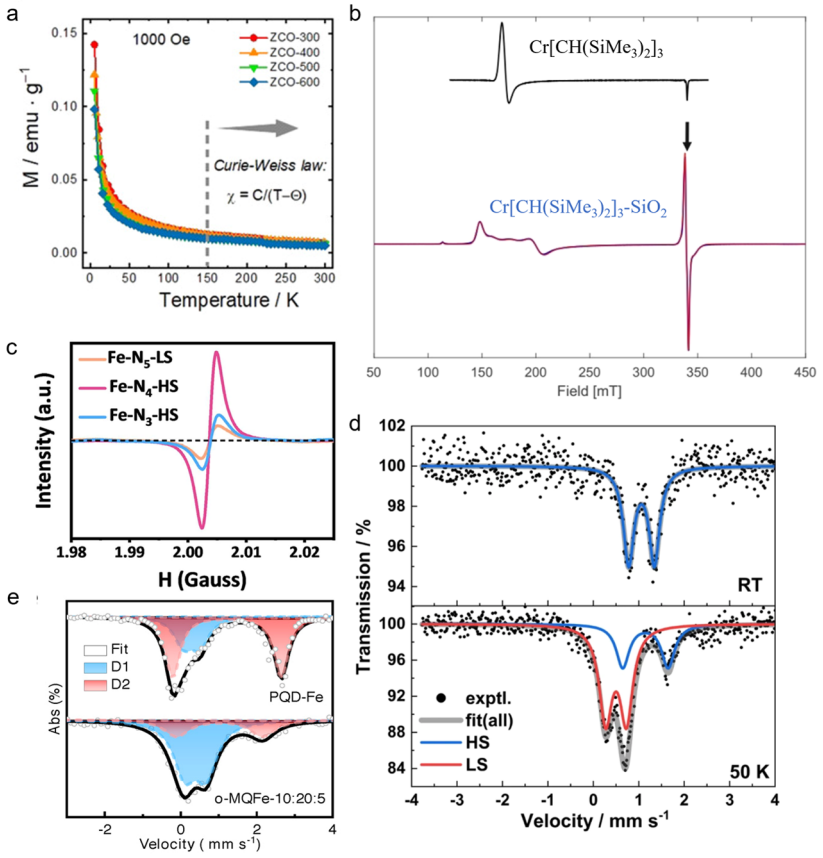

Figure 5. a Temperature-dependent magnetization of the $ZnCo_2O_4$ spinel oxides. Reprinted with permission from Reference [38]. Copyright 2021 Wiley-VCH. **b** 9.5 GHz CW EPR spectra of $Cr[CH(SiMe_3)_2]_3$ (black) and $Cr[CH(SiMe_3)_2]_3$-SiO_2 (blue), and simulation (red) of the two high spin (weighting factors 73.8% and 21.9%) and low spin (weighting factor 4.3%) Cr^{3+} species. Reprinted with permission under a CC-BY 4.0 license from Reference [51]. Copyright 2023 Wiley-VCH. **c** EPR spectra of Fe−N−C with different spin states. Reprinted with permission from Reference [52]. Copyright 2022 Elsevier Ltd. **d** ^{57}Fe Mössbauer spectra at room temperature and 50 K, respectively. Reprinted with permission under a CC-BY 4.0 license from Reference [57]. Copyright 2024 Springer Nature. **e** ^{57}Fe Mössbauer spectroscopy of PQD-Fe and o-MQFe-10:20:5. Reprinted with permission from Reference [37]. Copyright 2022 Wiley-VCH.

magneton). When calculating the spin state volume ratio of metal ions, we can use the formula $\mu_{eff} = g\mu_B * S_{eff}$ (g is the Lande factor, S_{eff} is the effective spin quantum number) Through VSM characterization of cobalt-based spinel oxides (Figure 5a), the Co^{3+} spin state can change from low spin to high spin with the increase of calcination temperature.[38]

3.2. Electron Paramagnetic Resonance

EPR is a technique that detects resonance phenomena associated with unpaired electrons in a substance.[49] However, its application is limited to paramagnetic materials and ferromagnetic materials. By analyzing the EPR spectra, we can investigate phenomena such as spin−lattice relaxation, spin−spin coupling, and spin−orbit coupling.[50] For instance, Figure 5b shows the EPR spectra of $Cr[CH(SiMe_3)_2]_3$ and $Cr[CH(SiMe_3)_2]_3$-SiO_2 to explore the spin-dependent electronic structure of Cr^{3+}.[51] The spectrum of $Cr[CH(SiMe_3)_2]_3$ (black) reveals a single S = 3/2 Cr^{3+} species with a pure axisymmetric zero-field splitting tensor (E/D = 0), indicating a pure high spin (S = 3/2). In contrast, the two spectral signals of $Cr[CH(SiMe_3)_2]_3$-SiO_2 (blue) demonstrate the presence of both high spin (100−250 mT) and low spin (S = 1/2; 300−400 mT) Cr^{3+}. Additionally, Figure 5c also shows the ERP spectrum of the Fe−N−C single atom catalyst, where the relative number of unpaired electrons is inferred from the intensity of the peak.[52]

3.3. Mössbauer Spectroscopy

Mössbauer spectroscopy is a technique that utilizes the recoilless resonance absorption effect of atomic nuclei to measure the interaction between the Mössbauer nucleus and hyperfine field. This method is used to study the valence state, spin state, coordination environment and phase information on active metals. Mössbauer spectroscopy of Fe is the most widely applied, typically providing insights into magnetic dipole interactions, electric quadrupole interactions and electric monopole interactions.[53−56] By fitting the Mössbauer spectroscopy, the quadrupole splitting and isomer shift can be given, and the relevant information on Fe ions can be determined based on these data.[32,37] Compared to the high spin state, the low spin states of both Fe^{2+} and Fe^{3+} exhibit lower isomer shifts. Additionally, low spin Fe^{2+} compounds display lower quadrupole splitting, while low spin Fe^{3+} compounds show higher quadrupole splitting. Figure 5d shows the Mössbauer spectra of $[Fe(BPND)(Ag(CN)_2)_2]\cdot 3CHCl_3$ at room temperature and 50 K.[57] At room temperature, the spectrum has double peaks, with an isomer shift of 1.061 mm s^{-1} and a quadrupole splitting of 0.565 mm s^{-1}, indicating that all Fe^{2+} are in a high spin state. At 50 K, an additional double peak appears corresponding to the low-spin state of Fe^{2+}, indicating that some Fe^{2+} undergoes a spin-state transition. The Fe−O−Ti ligand-mediated spin-state transition strategy was successfully verified by Mössbauer

https://doi.org/10.1021/acsmaterialsau.4c00092
ACS Mater. Au 2025, 5, 253−267

spectroscopy.[37] As shown in Figure 5e, the D1 and D2 peaks can be attributed to the intermediate spin and low spin structures of Fe^{3+}. And the D1 area of o-MQFe-10:20:5 (72.6%) is higher than that of PQD-Fe (34.6%), confirming the low spin transition to intermediate spin of Fe^{3+}.

3.4. X-ray Absorption Spectroscopy

XAS is frequently employed to analyze the oxidation state and coordination environment of catalysts and is particularly effective in characterizing metal spin states.[58] The characteristic shape and splitting of the lower energy front edge peak in X-ray absorption near-edge structure (XANES) provide insights into the local coordination field and spin state of the metal.[59] For instance, Huang et al. conducted XAS analyses on the Co L-edge and O K-edge of a series of $Co_xMn_{1-x}O_y$ oxides with varying compositions and other Co-based oxides (Figure 6a-b).[60] The content of the high-spin state was ranked by the intensity ratio of the L_3 and L_2 edges and was correlated with the OER performance (Figure 6c). Low spin Co^{3+} is more conducive to surface reconstruction of oxides and enhances OER performance under acidic conditions. XAS spectra also confirm the different spin states of Co^{3+} in $LaCoO_3$ epitaxial films with varying orientations (Figure 6d).[61] The weakest Co L_3 edge peak intensity in $LaCoO_3$ (100) indicates the highest volume ratio of Co^{3+} in the intermediate-spin state.

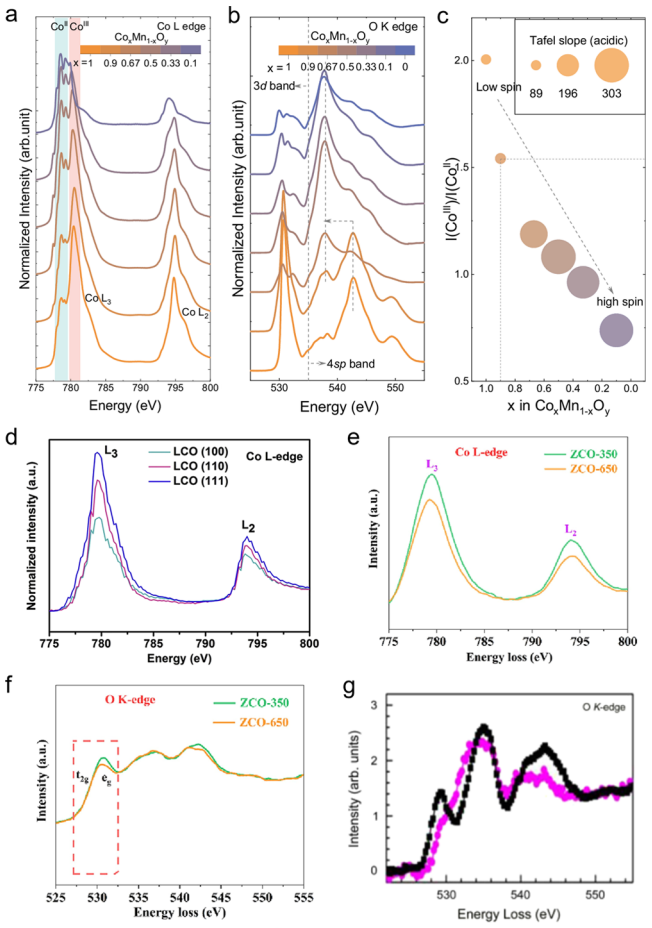

Figure 6. a Co L-edge XAS spectra for $Co_xMn_{1-x}O_y$. **b** O K-edge XAS spectra for $Co_xMn_{1-x}O_y$. **c** Correlations between Tafel slope and $I(Co^{III})/I(Co^{II})$. Reprinted with permission under a CC-BY 4.0 license from Reference [60]. Copyright 2024 Springer Nature. **d** Co L-edge XAS spectra for $LaCoO_3$ (100), (110), and (111) films. Reprinted with permission from Reference [61]. Copyright 2017, Elsevier Inc. **e** Co L-edge and **f** O K-edge EELS spectra of ZCO-350 and ZCO-650. Reprinted with permission from Reference [67]. Copyright 2023 Elsevier B.V. **g** O K-edge EELS spectra were recorded from the center (magenta) and edge (black) of the $LaCoO_3$. Reprinted with permission from Reference [65]. Copyright 2019 American Physical Society.

3.5. Electron Energy Loss Spectroscopy

EELS is a technique that measures the change in the kinetic energy of electrons after interacting with the materials. It is sensitive to the local structure of materials and can effectively characterize the local structural changes induced by spin state transitions.[62−66] Figure 6e and Figure 6f show the electron energy loss spectrum of $ZnCo_2O_4$.[67] The Co L-edge spectrum is dominated by Co $2p$-$3d$ transitions, with the two peaks corresponding to the L_3 edge and L_2 edge, respectively. The shape of the L_3 edge spectrum is strongly influenced by Co $3d$-$3d$ interaction and the degree of hybridization between the Co $3d$ and O $2p$ orbital. The decrease in intensity indicates that a portion of the Co e_g orbital has been filled, resulting in the formation of the intermediate-spin state Co^{3+}. The reduction in the O K-edge spectrum prepeak intensity suggests a spin state transition of Co^{3+} from low spin to intermediate spin, where electrons are redistributed, with some t_{2g} electrons occupying the e_g orbital. EELS also distinguishes between the spin states of Co^{3+} in the bulk and surface phases of $LaCoO_3$. The prepeak around 530 eV in the O K-edge spectrum is closely associated with the spin state of $LaCoO_3$, with a lower prepeak intensity corresponding to a higher spin state of Co^{3+} (Figure 6g).[65]

3.6. Modeling and Calculations

In magnetic analysis, theoretical modeling and calculations help to understand and predict the structure, thereby helping to explore the reaction mechanism.[68] The commonly used computational simulation method is the first-principles calculation based on DFT. Wang et al. calculated that the introduction of single-atom W delocalizes the spin state of Ni, resulting in an increase in the d electron density of Ni. This optimizes the adsorption/desorption process of hydrogen and oxygen intermediates, thereby accelerating the thermodynamics and kinetics of the hydrogen evolution reaction and OER.[69] Tang et al. calculated the catalytic activity and stability of Fe−N−C catalysts with different axial coordination functional groups. The results showed that low-spin pyridine-type FeN_4 has excellent acid resistance and high oxygen reduction reaction (ORR) activity.[70]

4. PROGRESS IN SPIN RESEARCH IN ELECTROCHEMISTRY

The spin configuration of a catalyst has been demonstrated to significantly influence its electrocatalytic activity.[68] Recent developments in spin catalysis mechanisms, such as spin polarization, spin−orbit coupling, and spin pinning effects, have rapidly advanced the field.[71] As a result, there is an increasing need to summarize these various mechanisms to further guide the synthesis of electrocatalytic materials with controllable spin states.

4.1. Influence of Active Site Spin on *d*-Band Center and Adsorption Energy

The adsorption and desorption energy of reactants and intermediates on metal active sites are crucial in determining the electron transfer efficiency during electrocatalysis, directly impacting the overall electrocatalytic performance. According to

https://doi.org/10.1021/acsmaterialsau.4c00092
ACS Mater. Au 2025, 5, 253−267

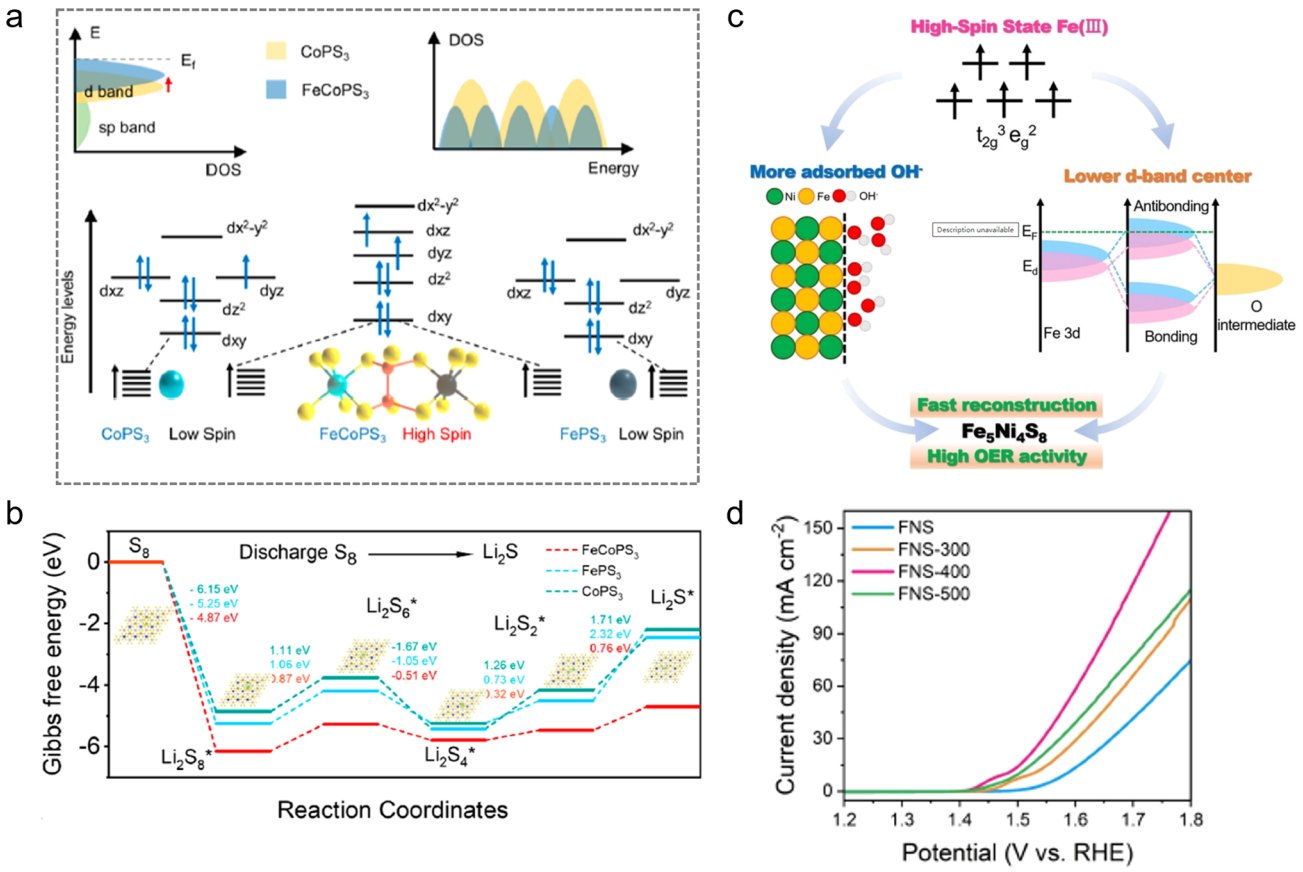

Figure 7. a Electronic configurations of the 3*d* orbital for $CoPS_3$, $FePS_3$, and $FeCoPS_3$. **b** Gibbs free energy on $CoPS_3$, $FePS_3$, and $FeCoPS_3$ catalysts. **c** Schematic diagram of the enhanced OER performance of Fe with high spin state. Reprinted with permission from Reference [72]. Copyright 2023, American Chemical Society. **d** CV curves comparison of the OER performance indicators of different samples. Reprinted with permission from Reference [73]. Copyright 2023 Wiley-VCH.

the Sabatier principle, the interaction between the catalyst surface and the reactants should be neither too strong nor too weak. The *d*-band theory proposed by Nørskov et al. further elaborates that the energy level of the *d*-band center determines the degree to which the antibonding energy band is filled with electrons, thereby determining the stability and strength of adsorption bonding. Recent studies have demonstrated that different spin states can affect the energy level of the *d*-band center.[72,73] For example, Li et al. synthesized $FeCoPS_3$ via a synchronous phosphorization and sulfidation method, resulting in notable orbital splitting and a high-spin configuration, which increases the number of unpaired electrons in the 3*d* orbital (Figure 7**a-c**).[72] This unique electronic structure enhances charge transfer and shifts the *d*-band center, thereby changing the adsorption energy and potential reaction pathways of lithium polysulfide. Sun et al. achieved a transformation of the Fe low spin to the high spin in pentlandite.[73] Theoretical calculations show that the high spin Fe has a lower *d*-band center, which optimizes the adsorption of active intermediates and exhibits an ultralow OER overpotential (245 mV @ 10 mA cm^{-2}) (Figure 7d).

4.2. Spin Effects Affect Electrocatalytic Kinetics

The spin effect influencing electrocatalytic kinetics is particularly significant in oxygen electrocatalysis.[74−78] This is because the type of oxygen molecule involved in these processes is crucial to the catalytic reaction.[77] Typically, singlet oxygen-containing molecular compounds (all electron spins are paired, and the total quantum number is 0) and triplet oxygen molecules (there are two unpaired electrons, with a total quantum number of 1) are present during the oxygen electrocatalytic process, and the interconversion between these two forms is governed by electron spin restrictions (Figure 8a). Triplet oxygen molecules possess higher spin angular momentum, making their energy 0.8 eV lower than that of singlet oxygen. Therefore, in oxygen electrocatalysis, the electron spin configuration of the catalyst's active center can be adjusted to modulate its electron spin interactions with reaction intermediates. At present, the research on the effect of spin on electrocatalytic kinetics and the enhancement of catalytic performance can be divided into two categories: spin catalysis and magnetic field catalysis (Figure 8b). Among them, magnetic field enhancement can be divided into external magnetic field and internal magnetic field.

4.2.1. Adjust the e_g Electrons Occupied. The occupation of the e_g orbital electron is primarily relevant in transition metal compounds, including perovskite oxides,[79−81] spinel oxides,[38,82,83] and metal chalcogenides.[84] Due to the crystal field effect, the *d* orbital of the ion at the octahedral site is split into three lower-energy t_{2g} orbitals and two higher-energy e_g orbitals.[85] In a strong crystal field, the six electrons of the Co^{3+} ion will occupy the t_{2g} orbital in pairs, resulting in a low-spin state.[26,86] In contrast, under a weak crystal field, the *d* electrons will follow Hund's rule, occupying the orbit as many as possible to form a high-spin state.[87] When the crystal field energy is intermediate, the spin state can shift to a intermediate spin state (Figure 8c).[88] Studies have indicated that there is a

https://doi.org/10.1021/acsmaterialsau.4c00092
ACS Mater. Au 2025, 5, 253−267

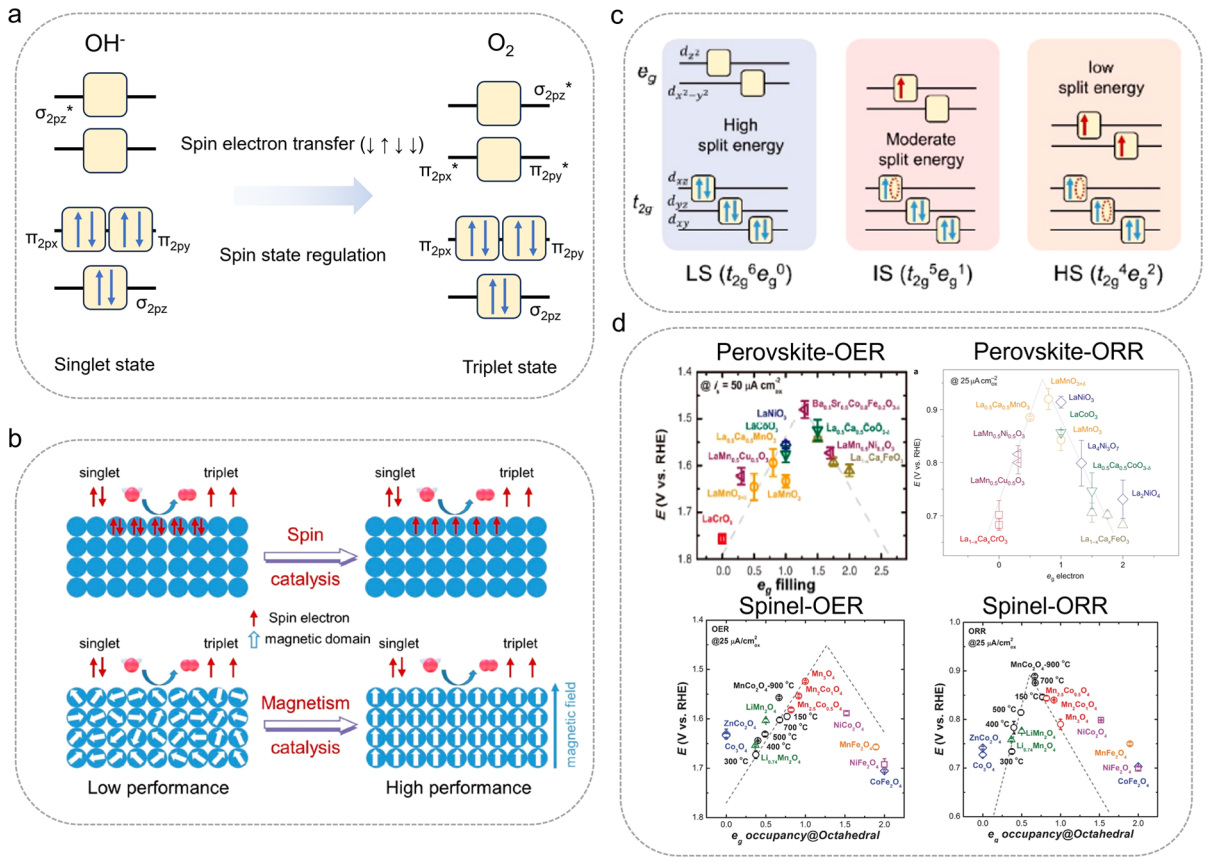

Figure 8. a The electronic configurations of singlet OH^- and triplet O_2. **b** Schematic diagrams of spin catalysis and magnetism catalysis. **c** The low spin (LS), intermediate spin (IS), and high spin (HS) of Co^{3+}. Reprinted with permission from Reference [88]. Copyright 2023 American Chemical Society. **d** Volcanic map between the e_g filling and OER/ORR activity. Reprinted with permission from Reference89 [90] [91]. Copyright 2011 Springer Nature Limited and American Association for the Advancement of Science and Copyright 2017 Wiley-VCH.

volcano-type relationship between the number of e_g electrons at the octahedral site and the OER/ORR activity (Figure 8d).[89−92] Wu et al. controlled the lattice orientation of $LaCoO_3$ film to cause different degrees of distortion of Co octahedron, thereby inducing the spin state of cobalt to transition from the low spin ($t_{2g}^6e_g^0$) to the intermediate spin ($t_{2g}^5e_g^1$), changing the electron filling rate of the e_g orbital, and thus obtaining better OER performance.[61]

4.2.2. External Magnetic Field Enhancement. Transition metal compounds contain numerous magnetic domains. When a magnetic field is introduced, these magnetic domains can be aligned in the same direction, thereby increasing the spin polarization rate. The formation of triplet oxygen requires the alignment of three electron spins in the same direction.[88] Spin polarization can optimize the selectivity and transfer efficiency of spin electrons, thereby reducing the kinetic energy barrier. Previous studies have shown that the OER activity of some magnetic materials is significantly enhanced under the action of an external magnetic field. In contrast, nonmagnetic catalysts do not show a significant enhancement effect (Figure 9**a-c**).[93] In addition, reducing the size of nanoparticles resulted in the formation of single-domain $CoFe_2O_4$, which did not exhibit enhanced catalytic performance under the magnetic field.[94] However, multidomain ferromagnetic $CoFe_2O_4$ aligns its magnetic domains in a magnetic field, promoting the arrangement of spin electrons to meet the formation requirements of triplet oxygen, thereby enhancing the OER activity (Figure 9**d-e**). By preparing NiFe films of varying thicknesses, it was observed that the magnetic domains were striped, with adjacent domains oriented in antiparallel directions (Figure 9**f-j**).[95] As the film thickness decreased, the width of the domain walls narrowed, and their area increased (Figure 9**f-g**). Under the influence of an external magnetic field, the domain walls disappeared. All NiFe films demonstrated enhanced OER activity after the application of a magnetic field. The spin polarization in the domain wall regions was weak, leading to poor OER activity. When an external magnetic field was applied, all domains aligned in the same direction, the domain walls vanished, spin polarization was strengthened, and OER activity improved (Figure 9h). Thus, the introduction of an external magnetic field can regulate the spin state of the catalyst, enhance spin polarization, and accelerate spin-related OER reactions (Figure 9**i-j**).

4.2.3. Internal Magnetic Field Enhancement. While external magnetic fields can enhance spin polarization, catalytic activity significantly diminishes once the field is removed, limiting its commercial application in technologies such as fuel cells. To overcome this limitation, the intrinsic magnetic properties of the catalyst itself can be utilized to generate an internal magnetic field, thereby accelerating spin-related oxygen electrocatalytic reactions. This approach requires a heterostructure composed of two components: a ferromagnetic (FM) material (magnetic layer) that generates the internal magnetic field, and a catalyst (catalytic layer) responsible for electrocatalysis, which is so-called spin pinning.[96,97] The spin pinning effect at the interface can align the spin direction, thereby

https://doi.org/10.1021/acsmaterialsau.4c00092
ACS Mater. Au 2025, 5, 253−267

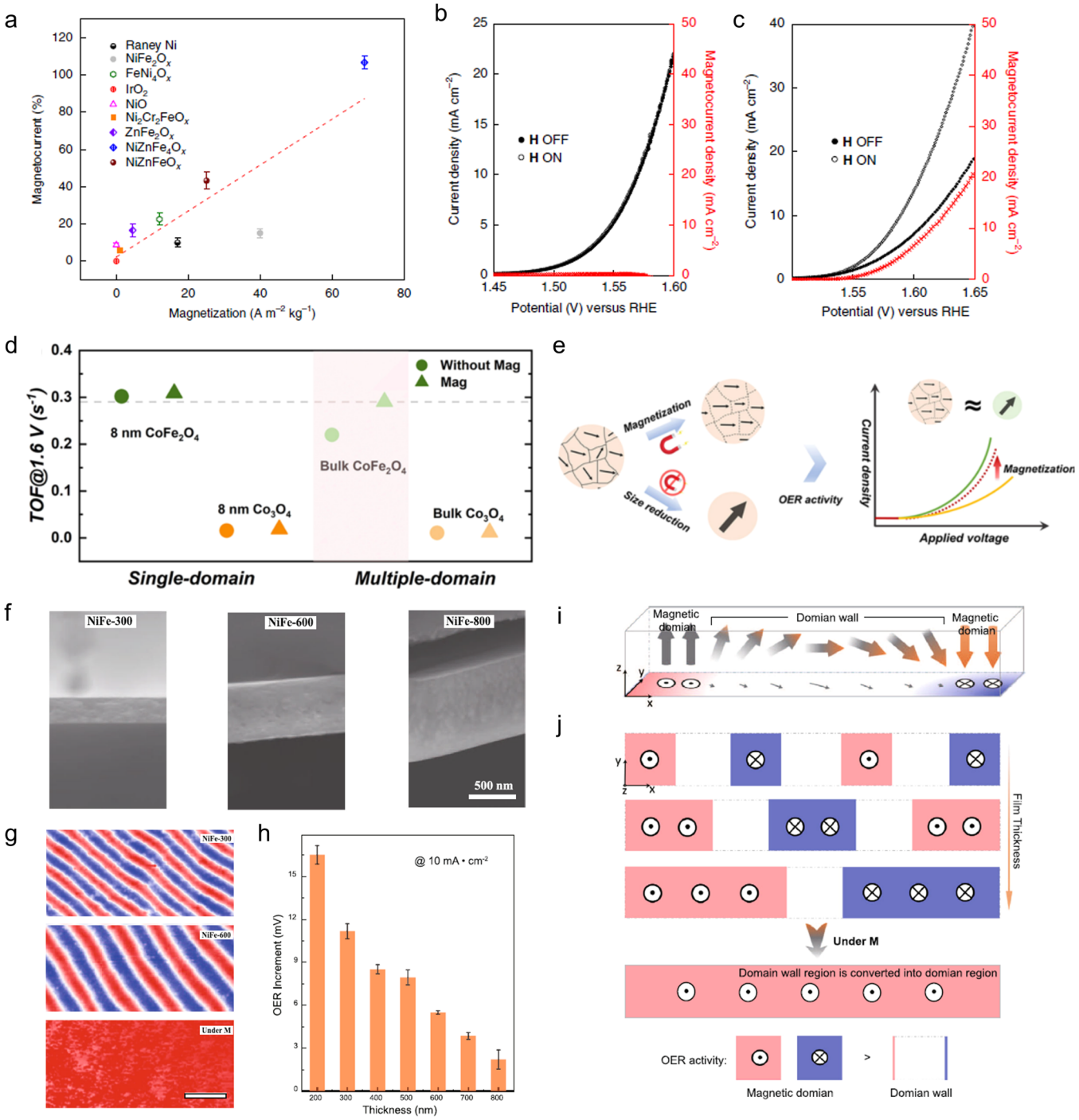

Figure 9. a The linear relationship between magnetization and magneto-current. CV curves of **b** IrO_2, and **c** $NiZnFe_4O_x$ with the external magnetic field turned on and off. Reprinted with permission from Reference [93]. Copyright 2019 Springer Nature. **d** The turnover frequency (TOF) values of 8 nm $CoFe_2O_4$, bulk $CoFe_2O_4$ and Co_3O_4 with/without a magnetic field. **e** Schematic diagram of the OER activity increment of multidomain and single-domain catalysts under the action of an external magnetic field. Reprinted with permission from Reference [94]. Copyright 2023 Wiley-VCH. **f** Sectional views of NiFe-300, NiFe-600, and NiFe-800. **g** Zero-field magnetic force microscopy images of the magnetic domain configuration of NiFe-300 and NiFe-600, and the corresponding magnetized NiFe-600 films under a 2000 Oe in-plane magnetic field. **h** OER increment for NiFe films with increasing thickness from 200 to 800 nm. **i** The directions of the magnetic moments of adjacent domains and the domain walls between them. **j** Magnetic domain area and domain wall area in NiFe films with different film thicknesses. Reprinted with permission under a CC-BY 4.0 license from Reference [95]. Copyright 2023 Springer Nature.

enhancing spin selectivity and catalytic activity. Xu et al. pioneered the use of the spin pinning effect to enhance the OER activity at the interface of FM oxide and oxyhydroxide (OHD).[42] In an alkaline environment, the surface of metal sulfides undergoes reconstruction to form OHD, and the reconstructed $Co_{3-x}Fe_xO_4/Co(Fe)O_xH_y$ structure has higher OER activity than the original $Co_{3-x}Fe_xO_4$ (Figure 10**a-c**). This enhancement is attributed to the spin pinning at the interface between the FM substrate and the OHD layer. The internal magnetic field generated by the FM layer can align the spin

https://doi.org/10.1021/acsmaterialsau.4c00092
ACS Mater. Au 2025, 5, 253−267

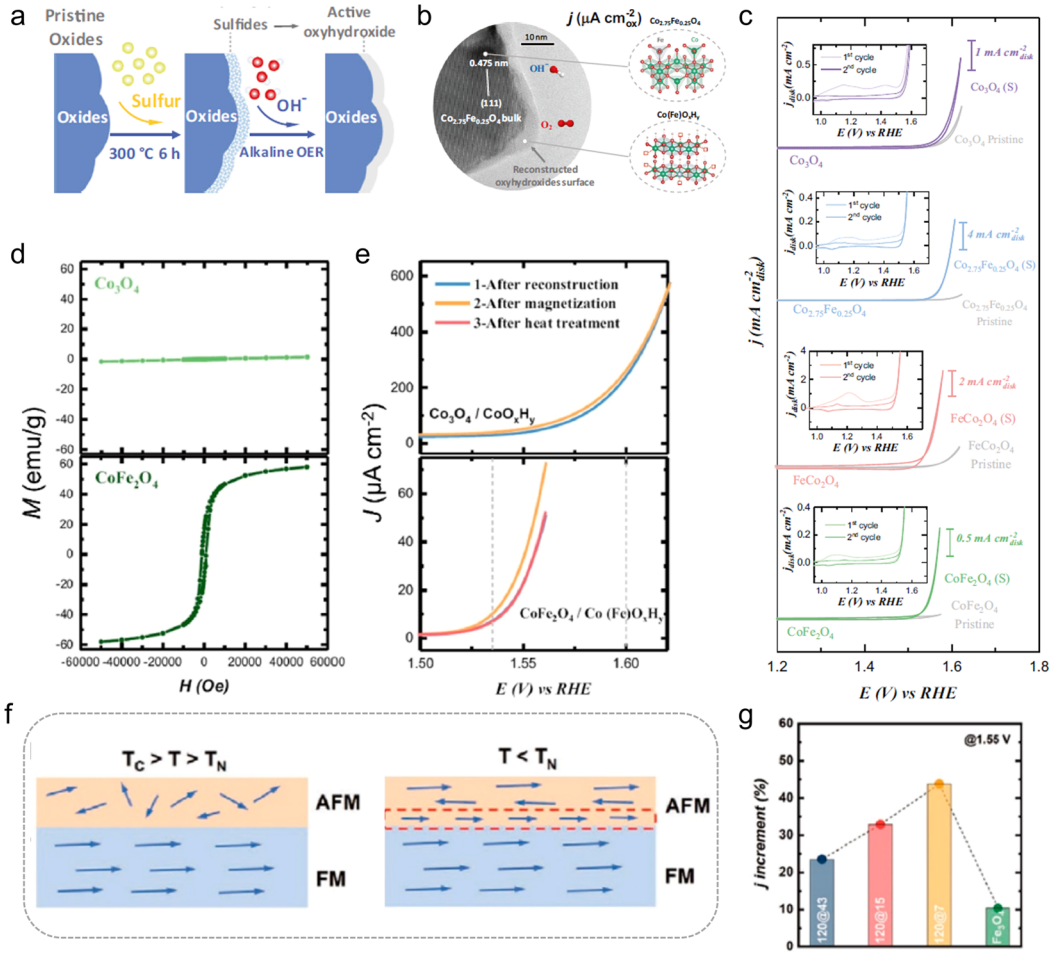

Figure 10. **a** Schematic diagram of a controllable reconstruction of oxides by controlled sulfurization. **b** The high-resolution transmission electron microscope (HRTEM) image of $Co_{2.75}Fe_{0.25}O_4$ after reconstruction. **c** The CV curves of $Co_xFe_{3-x}O_4$. Inset is the first and second CVs of sulfurized oxides. **d** The magnetic hysteresis loops of $Co_{3-x}Fe_xO_4$. **e** CV curves of $Co_{3-x}Fe_xO_4$. Reprinted with permission under a CC-BY 4.0 license from Reference [42]. Copyright 2021 Springer Nature. **f** Schematic diagram of FM-AFM coupling. **g** OER activity increment of Fe_3O_4 with different AFM shell thickness. Reprinted with permission from Reference [98]. Copyright 2021 Wiley-VCH.

direction of the catalyst layer at the interface through spin polarization. If the OHD layer is thin enough (about 4−5 nm), spin pinning can align the spins throughout the entire OHD layer. Figure 10**d-e** further proves that the enhanced spin alignment can improve the OER activity. Specifically, as the remanence of the FM substrate increases (Figure 10d), the internal magnetic field strengthens, resulting in more robust spin alignment and improved OER activity (Figure 10e). In addition, core−shell catalysts can take advantage of ferromagnetic-antiferromagnetic (FM-AFM) coupling to enhance the internal magnetic field, thereby improving spin selectivity and catalytic activity.[98] When the temperature is higher than the Neel temperature (T_N) of the AFM shell ($T_C > T > T_N$), the shell transitions into a spin-disordered paramagnetic state (Figure 10f). Conversely, when $T < T_N$, the shell becomes AFM, and the spins at the interface couple with the spin alignment of the ferromagnetic core. This exchange bias effect provides strong evidence of AM-AFM coupling at the core−shell interface. The AM-AFM coupling at the interface enhances spin electron selectivity by aligning the spins within the shell (Figure 10f), which in turn improves OER activity (Figure 10g). In summary, leveraging the inherent magnetism of the catalyst to generate an internal magnetic field represents a promising strategy for enhancing oxygen electrocatalytic performance by improving spin selectivity. Nonetheless, further research is necessary to fully explore and optimize this approach for more efficient oxygen electrocatalytic reactions.

4.3. Influence of Magnetic Elements on *d*-Band Center of Noble Metals

Precious metal catalysts, such as Ir, Ru, and Pt, continue to be the cornerstone of oxygen electrocatalysis under acidic conditions due to their exceptional activity and stability.[99−101] However, the exploration of spin-enhanced catalysis has primarily focused on magnetic elements like Fe, Co, and Ni, rather than paramagnetic elements such as precious metals. To address this gap, Shao et al. employed a spin-polarization-mediated strategy to induce a net ferromagnetic moment in antiferromagnetic RuO_2 by doping it with manganese (Mn^{2+}, S = 5/2) (Figure 11**a-b**), thereby enhancing its OER activity in acidic electrolytes.[102] Element-selective X-ray magnetic circular dichroism (XMCD) revealed ferromagnetic coupling between Mn and Ru ions, consistent with the Goodenough-Kanamori rule (Figure 11**c-d**). The Mn-doped RuO_2 nanosheets demonstrated significant magnetic field-enhanced OER activity, achieving a minimal overpotential of 143 mV at a current density of 10 mA cm^{-2} (Figure 11e). Similarly, Cai et al. modified the electronic structure of Ir by doping magnetic Fe into the paramagnetic Ir lattice, achieving Fe 3*d*-Ir 5*d* orbital hybrid-

https://doi.org/10.1021/acsmaterialsau.4c00092
ACS Mater. Au 2025, 5, 253−267

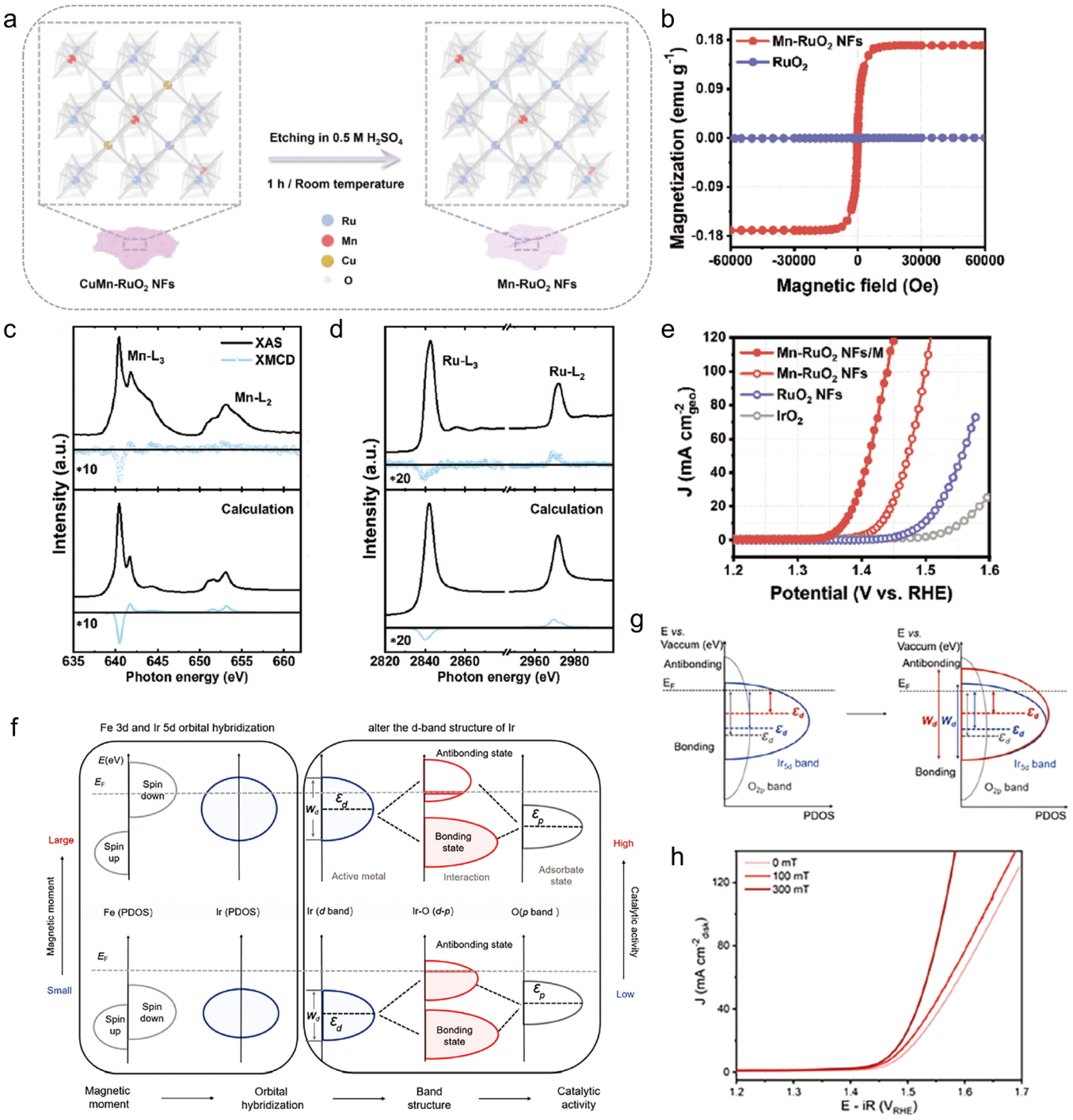

Figure 11. **a** Schematic illustration of the Mn-RuO_2 NFs preparation. **b** Magnetization hysteresis M−H loops of Mn-RuO_2 NFs and RuO_2. **c** Mn-$L_{2,3}$ XMCD and **d** Ru-$L_{2,3}$ XMCD of Mn-RuO_2 NFs at 300 K (top). **e** CV curves of Mn-RuO_2 NFs/M, Mn-RuO_2 NFs, RuO_2 NFs, and IrO_2. Reprinted with permission from Reference [102]. Copyright 2023 Wiley-VCH. **f** Illustration of the spin-induced orbital hybridization. Alloying Ir and Fe results in the hybridization of the Ir 5*d* and Fe 3*d* orbitals. Increasing the magnetic moment of Fe causes the spin splitting of the Fe 3*d* orbitals, shifting the spin-down band toward E_F. These two effects, i.e., spin splitting and orbital hybridization, alter the *d*-band structure of Ir at high magnetic moments, optimizing the binding strength with oxygen intermediates. **g** Variation of bonding/antibonding states of ε_d and W_d of Ir for Ir_3Fe and the O *p*-band center of the *O intermediate under different magnetic moments. **h** CVs of the Ir_3Fe-xmT aerogels in 0.5 M H_2SO_4 with a scan rate of 50 mV s^{-1}. Reprinted with permission from Reference [103]. Copyright 2024 Wiley-VCH.

ization (Figure 11f).[103] The increased magnetic moment induced by the spin splitting of the Fe 3*d* orbital caused the spin-down band to shift toward the Fermi level, thereby altering the *d*-band structure of Ir through orbital hybridization (Figure 11g). The resulting Ir−Fe aerogels exhibited outstanding OER electrocatalytic activity for water oxidation, with an overpotential as low as 236 mV at 10 mA cm^{-2} (Figure 11h). These studies demonstrate the potential of incorporating spin-polarization strategies in paramagnetic precious metal catalysts to enhance their electrocatalytic performance, opening new avenues for the development of high-performance catalysts under acidic conditions.

https://doi.org/10.1021/acsmaterialsau.4c00092
ACS Mater. Au 2025, 5, 253−267

5. SUMMARY AND PERSPECTIVE

This review systematically summarizes the regulation of spin states of catalytic active sites. We began by detailing various strategies for regulating active sites, including size regulation, defect engineering, doping engineering, magnetic field application, and metal−support interactions. Each of these approaches offers unique avenues for manipulating the electronic structure of active sites, thereby optimizing their catalytic performance. Next, we examined current spin characterization techniques, such as Vibrating Sample Magnetometry, Electron Paramagnetic Resonance, Mössbauer Spectroscopy, X-ray Absorption Spectroscopy, and Electron Energy Loss Spectroscopy. These advanced methods are crucial for identifying and understanding spin state transitions, providing deep insights into the relationship between spin states and catalytic activity. Finally, we summarize the current understanding of how spin effects enhance electrochemical performance and classify it into categories. These include spin polarization, spin−orbit coupling, and spin pinning, each contributing differently to the optimization of catalytic processes. Despite the significant progress, research on spin state transitions is still in its infancy. Future research directions might focus on the following aspects:

1) While existing techniques have provided valuable insights into the relationship between spin states and electrocatalytic performance, there remain significant challenges. One of the foremost challenges is the real-time detection of spin state changes during catalytic reactions. Current methods often fall short in capturing the dynamic nature of spin states under operational conditions. Therefore, advancing in situ and operando characterization techniques is critical. These methods would allow for real-time monitoring of spin states, offering a clearer understanding of how spin configurations evolve during reactions and directly influencing catalyst design.
2) Industrial electrocatalysis continues to rely heavily on noble metal catalysts due to their exceptional stability and activity. However, research on spin regulation within noble metal-based materials is relatively underdeveloped compared to transition metal systems. Future studies should focus on exploring how spin states can be manipulated in noble metal catalysts, potentially leading to breakthroughs in catalyst efficiency and cost-effectiveness. Understanding and controlling spin effects in these materials could revolutionize their application in industrial electrocatalysis, particularly under harsh conditions where stability is paramount.
3) Another promising direction involves the integration of concepts from spintronics into catalysis. By harnessing spin-polarized currents or magnetic effects, it may be possible to create next-generation catalysts with unprecedented control over reaction pathways. This interdisciplinary approach could open up new possibilities for energy conversion technologies, offering catalysts that are not only more efficient but also more selective and tunable.

In conclusion, while the field of spin state transitions in electrocatalysis is still emerging, it holds tremendous potential for advancing the design of high-performance catalysts. We hope this review not only highlights the current achievements but also inspires future research that will pave the way for the rational design of spin-regulated electrocatalysts. By addressing the challenges outlined and exploring new frontiers, the field can make significant strides toward more efficient and sustainable energy conversion technologies.

AUTHOR INFORMATION

Corresponding Author

Bin Cai − *School of Chemistry and Chemical Engineering, Shandong University, 250100 Jinan, China;* orcid.org/0000-0002-3263-0395; Email: bin.cai@sdu.edu.cn

Author

Cunyuan Gao − *School of Chemistry and Chemical Engineering, Shandong University, 250100 Jinan, China*

Complete contact information is available at: https://pubs.acs.org/10.1021/acsmaterialsau.4c00092

Author Contributions

CRediT: **Cunyuan Gao** conceptualization, formal analysis, writing - original draft. **Bin Cai** conceptualization, funding acquisition, writing - review & editing.

Notes

The authors declare no competing financial interest.

ACKNOWLEDGMENTS

This work was supported by the National Natural Science Foundation of China (Grant No. 22174087), Natural Science Foundation of Shandong Province (ZR2022QE001, ZR2023YQ039), and Taishan Scholar Foundation of Shandong Province (tsqn202211042).

REFERENCES

(1) Turner, J. A. Sustainable Hydrogen Production. *Science* **2004**, *305*, 972−974.
(2) Chu, S.; Majumdar, A. Opportunities and challenges for a sustainable energy future. *Nature* **2012**, *488*, 294−303.
(3) Seh, Z. W.; Kibsgaard, J.; Dickens, C. F.; Chorkendorff, I.; Nørskov, J. K.; Jaramillo, T. F. Combining theory and experiment in electrocatalysis: Insights into materials design. *Science* **2017**, *355*, No. eaad4998.
(4) Whittingham, M. S. Introduction: Batteries. *Chem. Rev.* **2014**, *114*, 11413−11413.
(5) Cheng, F.; Chen, J. Metal−air Batteries: from Oxygen Reduction Electrochemistry to Cathode Catalysts. *Chem. Soc. Rev.* **2012**, *41*, 2172−2192.
(6) Li, Y.; Dai, H. Recent Advances in Zinc−Air Batteries. *Chem. Soc. Rev.* **2014**, *43*, 5257−5275.
(7) Wang, Z.-L.; Xu, D.; Xu, J.-J.; Zhang, X.-B. Oxygen Electrocatalysts in Metal−AIr Batteries: from Aqueous to Nonaqueous Electrolytes. *Chem. Soc. Rev.* **2014**, *43*, 7746−7786.
(8) Sakakura, T.; Choi, J.-C.; Yasuda, H. Transformation of Carbon Dioxide. *Chem. Rev.* **2007**, *107*, 2365−2387.
(9) Ozden, A.; García de Arquer, F. P.; Huang, J. E.; Wicks, J.; Sisler, J.; Miao, R. K.; O'Brien, C. P.; Lee, G.; Wang, X.; Ip, A. H.; Sargent, E. H.; Sinton, D. Carbon-efficient carbon dioxide electrolysers. *Nat. Sustain.* **2022**, *5*, 563−573.
(10) Chen, J. G.; Crooks, R. M.; Seefeldt, L. C.; Bren, K. L.; Bullock, R. M.; Darensbourg, M. Y.; Holland, P. L.; Hoffman, B.; Janik, M. J.; Jones, A. K.; Kanatzidis, M. G.; King, P.; Lancaster, K. M.; Lymar, S. V.; Pfromm, P.; Schneider, W. F.; Schrock, R. R. Beyond fossil fuel−driven nitrogen transformations. *Science* **2018**, *360*, No. eaar6611.
(11) Tang, C.; Qiao, S.-Z. How to Explore Ambient Electrocatalytic Nitrogen Reduction Reliably and Insightfully. *Chem. Soc. Rev.* **2019**, *48*, 3166−3180.
(12) Pérez-Ramírez, J.; López, N. Strategies to break linear scaling relationships. *Nat. Catal.* **2019**, *2*, 971−976.

(13) Bligaard, T.; Nørskov, J. K.; Dahl, S.; Matthiesen, J.; Christensen, C. H.; Sehested, J. The Brønsted−Evans−Polanyi Relation and the Volcano Curve in Heterogeneous Catalysis. *J. Catal.* **2004**, *224*, 206−217.
(14) Hammer, B.; Norskov, J. K. Why gold is the noblest of all the metals. *Nature* **1995**, *376*, 238−240.
(15) Calle-Vallejo, F.; Tymoczko, J.; Colic, V.; Vu, Q. H.; Pohl, M. D.; Morgenstern, K.; Loffreda, D.; Sautet, P.; Schuhmann, W.; Bandarenka, A. S. Finding optimal surface sites on heterogeneous catalysts by counting nearest neighbors. *Science* **2015**, *350*, 185−189.
(16) Du, W.; Yan, C.; Gao, M.; Chen, J.; Gao, P.; Yu, X.; Jiang, Y.; Sun, W.; Liu, Y.; Gao, M.; Xi, S.; Pan, H. Tuning coordination environment of iron ions to ensure ultra-high pseudocapacitive capability in iron oxide. *Nano Res.* **2023**, *16*, 6914−6921.
(17) Zhao, J.; Zhang, Y.; Zhuang, Z.; Deng, Y.; Gao, G.; Li, J.; Meng, A.; Li, G.; Wang, L.; Li, Z.; Wang, D. Tailoring d−p Orbital Hybridization to Decipher the Essential Effects of Heteroatom Substitution on Redox Kinetics. *Angew. Chem., Int. Ed.* **2024**, *63*, No. e202404968.
(18) Medford, A. J.; Vojvodic, A.; Hummelshøj, J. S.; Voss, J.; Abild-Pedersen, F.; Studt, F.; Bligaard, T.; Nilsson, A.; Nørskov, J. K. From the Sabatier Principle to a Predictive Theory of Transition-Metal Heterogeneous Catalysis. *J. Catal.* **2015**, *328*, 36−42.
(19) Zhao, Z.-J.; Liu, S.; Zha, S.; Cheng, D.; Studt, F.; Henkelman, G.; Gong, J. Theory-guided design of catalytic materials using scaling relationships and reactivity descriptors. *Nat. Rev. Mater.* **2019**, *4*, 792−804.
(20) Jiao, S.; Fu, X.; Huang, H. Descriptors for the Evaluation of Electrocatalytic Reactions: d-Band Theory and Beyond. *Adv. Funct. Mater.* **2022**, *32*, No. 2107651.
(21) Huang, P.; Meng, M.; Zhou, G.; Wang, P.; Wei, W.; Li, H.; Huang, R.; Liu, F.; Liu, L. Dynamic orbital hybridization triggered spin-disorder renormalization via super-exchange interaction for oxygen evolution reaction. *P. Natl. Acad. Sci. Usa* **2023**, *120*, No. e2219661120.
(22) Lin, C.-C.; Liu, T.-R.; Lin, S.-R.; Boopathi, K. M.; Chiang, C.-H.; Tzeng, W.-Y.; Chien, W.-H. C.; Hsu, H.-S.; Luo, C.-W.; Tsai, H.-Y.; Chen, H.-A.; Kuo, P.-C.; Shiue, J.; Chiou, J.-W.; Pong, W.-F.; Chen, C.-C.; Chen, C.-W. Spin-Polarized Photocatalytic CO_2 Reduction of Mn-Doped Perovskite Nanoplates. *J. Am. Chem. Soc.* **2022**, *144*, 15718−15726.
(23) Luo, S.; Elouarzaki, K.; Xu, Z. J. Electrochemistry in Magnetic Fields. *Angew. Chem., Int. Ed.* **2022**, *61*, No. e202203564.
(24) Zhang, A.; Liang, Y.; Zhang, H.; Geng, Z.; Zeng, J. Doping Regulation in Transition Metal Compounds for Electrocatalysis. *Chem. Soc. Rev.* **2021**, *50*, 9817−9844.
(25) Li, S.; Xia, L.; Li, J.; Chen, Z.; Zhang, W.; Zhu, J.; Yu, R.; Liu, F.; Lee, S.; Zhao, Y.; Zhou, L.; Mai, L. Tuning Structural and Electronic Configuration of FeN via External S for Enhanced Oxygen Reduction Reaction. *Energy Environ. Mater.* **2024**, *7*, No. e12560.
(26) Zhou, S.; Miao, X.; Zhao, X.; Ma, C.; Qiu, Y.; Hu, Z.; Zhao, J.; Shi, L.; Zeng, J. Engineering electrocatalytic activity in nanosized perovskite cobaltite through surface spin-state transition. *Nat. Commun.* **2016**, *7*, No. 11510.
(27) Qian, D.; Hinuma, Y.; Chen, H.; Du, L.-S.; Carroll, K. J.; Ceder, G.; Grey, C. P.; Meng, Y. S. Electronic Spin Transition in Nanosize Stoichiometric Lithium Cobalt Oxide. *J. Am. Chem. Soc.* **2012**, *134*, 6096−6099.
(28) Zhao, Y.; Jia, X.; Chen, G.; Shang, L.; Waterhouse, G. I. N.; Wu, L.-Z.; Tung, C.-H.; O'Hare, D.; Zhang, T. Ultrafine NiO Nanosheets Stabilized by TiO_2 from Monolayer NiTi-LDH Precursors: An Active Water Oxidation Electrocatalyst. *J. Am. Chem. Soc.* **2016**, *138*, 6517−6524.
(29) Huang, J.; Chen, J.; Yao, T.; He, J.; Jiang, S.; Sun, Z.; Liu, Q.; Cheng, W.; Hu, F.; Jiang, Y.; Pan, Z.; Wei, S. CoOOH Nanosheets with High Mass Activity for Water Oxidation. *Angew. Chem., Int. Ed.* **2015**, *54*, 8722−8727.
(30) Zhao, S.; Wang, Y.; Dong, J.; He, C.-T.; Yin, H.; An, P.; Zhao, K.; Zhang, X.; Gao, C.; Zhang, L.; Lv, J.; Wang, J.; Zhang, J.; Khattak, A. M.; Khan, N. A.; Wei, Z.; Zhang, J.; Liu, S.; Zhao, H.; Tang, Z. Ultrathin metal−organic framework nanosheets for electrocatalytic oxygen evolution. *Nat. Energy* **2016**, *1*, No. 16184.
(31) Yang, G.; Zhu, J.; Yuan, P.; Hu, Y.; Qu, G.; Lu, B.-A.; Xue, X.; Yin, H.; Cheng, W.; Cheng, J.; Xu, W.; Li, J.; Hu, J.; Mu, S.; Zhang, J.-N. Regulating Fe-spin state by atomically dispersed Mn-N in Fe-N-C catalysts with high oxygen reduction activity. *Nat. Commun.* **2021**, *12*, 1734.
(32) Li, J.; Sougrati, M. T.; Zitolo, A.; Ablett, J. M.; Oğuz, I. C.; Mineva, T.; Matanovic, I.; Atanassov, P.; Huang, Y.; Zenyuk, I.; Di Cicco, A.; Kumar, K.; Dubau, L.; Maillard, F.; Dražić, G.; Jaouen, F. Identification of durable and non-durable FeNx sites in Fe−N−C materials for proton exchange membrane fuel cells. *Nat. Catal.* **2021**, *4*, 10−19.
(33) Chen, Z.; Niu, H.; Ding, J.; Liu, H.; Chen, P.-H.; Lu, Y.-H.; Lu, Y.-R.; Zuo, W.; Han, L.; Guo, Y.; Hung, S.-F.; Zhai, Y. Unraveling the Origin of Sulfur-Doped Fe-N-C Single-Atom Catalyst for Enhanced Oxygen Reduction Activity: Effect of Iron Spin-State Tuning. *Angew. Chem., Int. Ed.* **2021**, *60*, 25404−25410.
(34) Huang, J.; Zhou, W.; Luo, X.; Ding, Y.; Peng, D.; Chen, M.; Zhou, H.; Hu, C.; Yuan, C.; Wang, S. Enhancing hydrogen evolution reaction of confined monodispersed $NiSe_{2-X}$ nanoparticles by high-frequency alternating magnetic fields. *Chem. Eng. J.* **2023**, *454*, No. 140279.
(35) Li, Y.; Cheng, C.; Han, S.; Huang, Y.; Du, X.; Zhang, B.; Yu, Y. Electrocatalytic Reduction of Low-Concentration Nitric Oxide into ammonia over Ru Nanosheets. *ACS Energy Lett.* **2022**, *7*, 1187−1194.
(36) Zhang, Y.; Liang, C.; Wu, J.; Liu, H.; Zhang, B.; Jiang, Z.; Li, S.; Xu, P. Recent Advances in Magnetic Field-Enhanced Electrocatalysis. *Acs Appl. Energy Mater.* **2020**, *3*, 10303−10316.
(37) Liu, Y.; Liu, X.; Lv, Z.; Liu, R.; Li, L.; Wang, J.; Yang, W.; Jiang, X.; Feng, X.; Wang, B. Tuning the Spin State of the Iron Center by Bridge-Bonded Fe-O-Ti Ligands for Enhanced Oxygen Reduction. *Angew. Chem., Int. Ed.* **2022**, *61*, No. e202117617.
(38) Sun, Y.; Ren, X.; Sun, S.; Liu, Z.; Xi, S.; Xu, Z. J. Engineering High-Spin State Cobalt Cations in Spinel Zinc Cobalt Oxide for Spin Channel Propagation and Active Site Enhancement in Water Oxidation. *Angew. Chem., Int. Ed.* **2021**, *60*, 14536−14544.
(39) Zhang, X.; Zhong, H.; Zhang, Q.; Zhang, Q.; Wu, C.; Yu, J.; Ma, Y.; An, H.; Wang, H.; Zou, Y.; Diao, C.; Chen, J.; Yu, Z. G.; Xi, S.; Wang, X.; Xue, J. High-spin Co^{3+} in cobalt oxyhydroxide for efficient water oxidation. *Nat. Commun.* **2024**, *15*, 1383.
(40) Miao, X.; Wu, L.; Lin, Y.; Yuan, X.; Zhao, J.; Yan, W.; Zhou, S.; Shi, L. The role of oxygen vacancies in water oxidation for perovskite cobalt oxide electrocatalysts: are more better? *Chem. Commun.* **2019**, *55*, 1442−1445.
(41) Yang, Y.; Zhang, L.; Hu, Z.; Zheng, Y.; Tang, C.; Chen, P.; Wang, R.; Qiu, K.; Mao, J.; Ling, T.; Qiao, S.-Z. The Crucial Role of Charge Accumulation and Spin Polarization in Activating Carbon-Based Catalysts for Electrocatalytic Nitrogen Reduction. *Angew. Chem., Int. Ed.* **2020**, *59*, 4525−4531.
(42) Wu, T.; Ren, X.; Sun, Y.; Sun, S.; Xian, G.; Scherer, G. G.; Fisher, A. C.; Mandler, D.; Ager, J. W.; Grimaud, A.; Wang, J.; Shen, C.; Yang, H.; Gracia, J.; Gao, H.-J.; Xu, Z. J. Spin pinning effect to reconstructed oxyhydroxide layer on ferromagnetic oxides for enhanced water oxidation. *Nat. Commun.* **2021**, *12*, 3634.
(43) Ren, X.; Wu, T.; Gong, Z.; Pan, L.; Meng, J.; Yang, H.; Dagbjartsdottir, F. B.; Fisher, A.; Gao, H.-J.; Xu, Z. J. The origin of magnetization-caused increment in water oxidation. *Nat. Commun.* **2023**, *14*, 2482.
(44) Zhou, G.; Wang, P.; Li, H.; Hu, B.; Sun, Y.; Huang, R.; Liu, L. Spin-state reconfiguration induced by alternating magnetic field for efficient oxygen evolution reaction. *Nat. Commun.* **2021**, *12*, 4827.
(45) Li, Z.; Wang, Z.; Xi, S.; Zhao, X.; Sun, T.; Li, J.; Yu, W.; Xu, H.; Herng, T. S.; Hai, X.; Lyu, P.; Zhao, M.; Pennycook, S. J.; Ding, J.; Xiao, H.; Lu, J. Tuning the Spin Density of Cobalt Single-Atom Catalysts for Efficient Oxygen Evolution. *ACS Nano* **2021**, *15*, 7105−7113.
(46) Tang, C.; Zheng, Y.; Jaroniec, M.; Qiao, S.-Z. Electrocatalytic Refinery for Sustainable Production of Fuels and Chemicals. *Angew. Chem., Int. Ed.* **2021**, *60*, 19572−19590.

https://doi.org/10.1021/acsmaterialsau.4c00092
ACS Mater. Au 2025, 5, 253−267

(47) Foner, S. Versatile and Sensitive Vibrating-Sample Magnetometer. *Rev. Sci. Instrum.* **1959**, *30*, 548−557.
(48) Mugiraneza, S.; Hallas, A. M. Tutorial: A Beginner's Guide to Interpreting Magnetic Susceptibility Data with the Curie-Weiss Law. *Commun. Phys.* **2022**, *5*, 95.
(49) Brückner, A. In Situ Electron Paramagnetic Resonance: A Unique Tool for Analyzing Structure−Reactivity Relationships in Heterogeneous Catalysis. *Chem. Soc. Rev.* **2010**, *39*, 4673−4684.
(50) Seifert, T. S.; Kovarik, S.; Juraschek, D. M.; Spaldin, N. A.; Gambardella, P.; Stepanow, S. Longitudinal and transverse electron paramagnetic resonance in a scanning tunneling microscope. *Sci. Adv.* **2020**, *6*, No. eabc5511.
(51) Ashuiev, A.; Giorgia Nobile, A.; Trummer, D.; Klose, D.; Guda, S.; Safonova, O. V.; Copéret, C.; Guda, A.; Jeschke, G. Active Sites in Cr(III)-Based Ethylene Polymerization Catalysts from Machine-Learning-Supported XAS and EPR Spectroscopy. *Angew. Chem., Int. Ed.* **2024**, *63*, No. e202313348.
(52) Xue, D.; Yuan, P.; Jiang, S.; Wei, Y.; Zhou, Y.; Dong, C.-L.; Yan, W.; Mu, S.; Zhang, J.-N. Altering the spin state of Fe-N-C through ligand field modulation of single-atom sites boosts the oxygen reduction reaction. *Nano Energy* **2023**, *105*, No. 108020.
(53) Bykova, E.; Dubrovinsky, L.; Dubrovinskaia, N.; Bykov, M.; McCammon, C.; Ovsyannikov, S. V.; Liermann, H. P.; Kupenko, I.; Chumakov, A. I.; Rüffer, R.; Hanfland, M.; Prakapenka, V. Structural complexity of simple Fe_2O_3 at high pressures and temperatures. *Nat. Commun.* **2016**, *7*, No. 10661.
(54) Kramm, U. I.; Lefèvre, M.; Larouche, N.; Schmeisser, D.; Dodelet, J.-P. Correlations between Mass Activity and Physicochemical Properties of Fe/N/C Catalysts for the ORR in PEM Fuel Cell via ^{57}Fe Mössbauer Spectroscopy and Other Techniques. *J. Am. Chem. Soc.* **2014**, *136*, 978−985.
(55) Kramm, U. I.; Ni, L.; Wagner, S. ^{57}Fe Mössbauer Spectroscopy Characterization of Electrocatalysts. *Adv. Mater.* **2019**, *31*, No. 1805623.
(56) Liu, W.; Zhang, L.; Liu, X.; Liu, X.; Yang, X.; Miao, S.; Wang, W.; Wang, A.; Zhang, T. Discriminating Catalytically Active FeN_x Species of Atomically Dispersed Fe−N−C Catalyst for Selective Oxidation of the C−H Bond. *J. Am. Chem. Soc.* **2017**, *139*, 10790−10798.
(57) Wu, X.-R.; Wu, S.-Q.; Liu, Z.-K.; Chen, M.-X.; Tao, J.; Sato, O.; Kou, H.-Z. Integrating spin-dependent emission and dielectric switching in Fe^{II} catenated metal-organic frameworks. *Nat. Commun.* **2024**, *15*, 3961.
(58) Glatzel, P.; Bergmann, U. High Resolution 1s Core Hole X-ray Spectroscopy in 3d Transition Metal Complexes—Electronic and Structural Information. *Coordin. Chem. Rev.* **2005**, *249*, 65−95.
(59) Cutsail, G. E., III; DeBeer, S. Challenges and Opportunities for Applications of Advanced X-ray Spectroscopy in Catalysis Research. *ACS Catal.* **2022**, *12*, 5864−5886.
(60) Huang, J.; Borca, C. N.; Huthwelker, T.; Yüzbasi, N. S.; Baster, D.; El Kazzi, M.; Schneider, C. W.; Schmidt, T. J.; Fabbri, E. Surface oxidation/spin state determines oxygen evolution reaction activity of cobalt-based catalysts in acidic environment. *Nat. Commun.* **2024**, *15*, 3067.
(61) Tong, Y.; Guo, Y.; Chen, P.; Liu, H.; Zhang, M.; Zhang, L.; Yan, W.; Chu, W.; Wu, C.; Xie, Y. Spin-State Regulation of Perovskite Cobaltite to Realize Enhanced Oxygen Evolution Activity. *Chem.* **2017**, *3*, 812−821.
(62) Xia, B.; Wang, T.; Ran, J.; Jiang, S.; Gao, X.; Gao, D. Optimized Conductivity and Spin States in N-Doped $LaCoO_3$ for Oxygen Electrocatalysis. *ACS Appl. Mater. Interfaces* **2021**, *13*, 2447−2454.
(63) Gulec, A.; Phelan, D.; Leighton, C.; Klie, R. F. Simultaneous First-Order Valence and Oxygen Vacancy Order/Disorder Transitions in $(Pr_{0.85}Y_{0.15})_{0.7}Ca_{0.3}CoO_{3-\delta}$ via Analytical Transmission Electron Microscopy. *ACS Nano* **2016**, *10*, 938−947.
(64) Klie, R. F.; Zheng, J. C.; Zhu, Y.; Varela, M.; Wu, J.; Leighton, C. Direct Measurement of the Low-Temperature Spin-State Transition in $LaCoO_3$. *Phys. Rev. Lett.* **2007**, *99*, No. 047203.
(65) Ma, C.; Lin, N.; Wang, Z.; Zhou, S.; Yu, H.; Lu, J.; Huang, H. Origin of spin-state crossover and electronic reconstruction at the surface of a $LaCoO_3$ nanoparticle. *Phys. Rev. B* **2019**, *99*, No. 115401.
(66) Lan, Q. Q.; Zhang, X. J.; Shen, X.; Yang, H. W.; Zhang, H. R.; Guan, X. X.; Wang, W.; Yao, Y.; Wang, Y. G.; Peng, Y.; Liu, B. G.; Sun, J. R.; Yu, R. C. Tuning the magnetism of epitaxial cobalt oxide thin films by electron beam irradiation. *Phys. Rev. Mater.* **2017**, *1*, No. 024403.
(67) Ren, L.; Wen, X.; Du, D.; Yan, Y.; Xu, H.; Zeng, T.; Shu, C. Engineering high-spin state cobalt cations in spinel $ZnCo_2O_4$ for spin channel propagation and electrocatalytic activity enhancement in Li-O_2 battery. *Chem. Eng. J.* **2023**, *462*, No. 142288.
(68) Zhang, Y.; Wu, Q.; Seow, J. Z. Y.; Jia, Y.; Ren, X.; Xu, Z. J. Spin States of Metal Centers in Electrocatalysis. *Chem. Soc. Rev.* **2024**, *53*, 8123−8136.
(69) Wang, Y.; Li, X.; Zhang, M.; Zhang, J.; Chen, Z.; Zheng, X.; Tian, Z.; Zhao, N.; Han, X.; Zaghib, K.; Wang, Y.; Deng, Y.; Hu, W. Highly Active and Durable Single-Atom Tungsten-Doped $NiS_{0.5}Se_{0.5}$ Nanosheet @ $NiS_{0.5}Se_{0.5}$ Nanorod Heterostructures for Water Splitting. *Adv. Mater.* **2022**, *34*, No. 2107053.
(70) Sun, F.; Li, F.; Tang, Q. Spin State as a Participator for Demetalation Durability and Activity of Fe−N−C Electrocatalysts. *J. Phys. Chem. C* **2022**, *126*, 13168−13181.
(71) Jiang, Y.; Yang, K.; Li, M.; Xu, D.; Ma, Z. Engineering the Spin Configuration of Electrocatalysts for Electrochemical Renewable Conversions. *Mater. Chem. Front.* **2024**, *8*, 528−552.
(72) Li, H.; Chuai, M.; Xiao, X.; Jia, Y.; Chen, B.; Li, C.; Piao, Z.; Lao, Z.; Zhang, M.; Gao, R.; Zhang, B.; Han, Z.; Yang, J.; Zhou, G. Regulating the Spin State Configuration in Bimetallic Phosphorus Trisulfides for Promoting Sulfur Redox Kinetics. *J. Am. Chem. Soc.* **2023**, *145*, 22516−22526.
(73) Du, Z.; Meng, Z.; Gong, X.; Hao, Z.; Li, X.; Sun, H.; Hu, X.; Yu, S.; Tian, H. Rapid Surface Reconstruction of Pentlandite by High-Spin State Iron for Efficient Oxygen Evolution Reaction. *Angew. Chem., Int. Ed.* **2024**, *63*, No. e202317022.
(74) Mtangi, W.; Tassinari, F.; Vankayala, K.; Vargas Jentzsch, A.; Adelizzi, B.; Palmans, A. R. A.; Fontanesi, C.; Meijer, E. W.; Naaman, R. Control of Electrons' Spin Eliminates Hydrogen Peroxide Formation During Water Splitting. *J. Am. Chem. Soc.* **2017**, *139*, 2794−2798.
(75) Jiao, Y.; Sharpe, R.; Lim, T.; Niemantsverdriet, J. W. H.; Gracia, J. Photosystem II Acts as a Spin-Controlled Electron Gate during Oxygen Formation and Evolution. *J. Am. Chem. Soc.* **2017**, *139*, 16604−16608.
(76) Chen, R. R.; Sun, Y.; Ong, S. J. H.; Xi, S.; Du, Y.; Liu, C.; Lev, O.; Xu, Z. J. Antiferromagnetic Inverse Spinel Oxide $LiCoVO_4$ with Spin-Polarized Channels for Water Oxidation. *Adv. Mater.* **2020**, *32*, No. 1907976.
(77) Sun, Y.; Sun, S.; Yang, H.; Xi, S.; Gracia, J.; Xu, Z. J. Spin-Related Electron Transfer and Orbital Interactions in Oxygen Electrocatalysis. *Adv. Mater.* **2020**, *32*, No. 2003297.
(78) Göhler, B.; Hamelbeck, V.; Markus, T. Z.; Kettner, M.; Hanne, G. F.; Vager, Z.; Naaman, R.; Zacharias, H. Spin Selectivity in Electron Transmission Through Self-Assembled Monolayers of Double-Stranded DNA. *Science* **2011**, *331*, 894−897.
(79) Qian, J.; Wang, T.; Zhang, Z.; Liu, Y.; Li, J.; Gao, D. Engineered spin state in Ce doped $LaCoO_3$ with enhanced electrocatalytic activity for rechargeable Zn-Air batteries. *Nano Energy* **2020**, *74*, No. 104948.
(80) Peña, M. A.; Fierro, J. L. G. Chemical Structures and Performance of Perovskite Oxides. *Chem. Rev.* **2001**, *101*, 1981−2018.
(81) Duan, Y.; Sun, S.; Xi, S.; Ren, X.; Zhou, Y.; Zhang, G.; Yang, H.; Du, Y.; Xu, Z. J. Tailoring the Co 3d-O 2p Covalency in $LaCoO_3$ by Fe Substitution To Promote Oxygen Evolution Reaction. *Chem. Mater.* **2017**, *29*, 10534−10541.
(82) Zhou, Y.; Sun, S.; Xi, S.; Duan, Y.; Sritharan, T.; Du, Y.; Xu, Z. J. Superexchange Effects on Oxygen Reduction Activity of Edge-Sharing $[Co_xMn_{1-x}O_6]$ Octahedra in Spinel Oxide. *Adv. Mater.* **2018**, *30*, No. 1705407.
(83) Sun, Y.; Liao, H.; Wang, J.; Chen, B.; Sun, S.; Ong, S. J. H.; Xi, S.; Diao, C.; Du, Y.; Wang, J.-O.; Breese, M. B. H.; Li, S.; Zhang, H.; Xu, Z. J. Covalency competition dominates the water oxidation structure−activity relationship on spinel oxides. *Nat. Catal.* **2020**, *3*, 554−563.

https://doi.org/10.1021/acsmaterialsau.4c00092
ACS Mater. Au 2025, 5, 253−267

(84) Zhang, J.-Y.; Yan, Y.; Mei, B.; Qi, R.; He, T.; Wang, Z.; Fang, W.; Zaman, S.; Su, Y.; Ding, S.; Xia, B. Y. Local Spin-State Tuning of Cobalt−Iron Selenide Nanoframes for the Boosted Oxygen Evolution. *Energy Environ. Sci.* **2021**, *14*, 365−373.
(85) Ahn, K. H.; Wu, X. W.; Liu, K.; Chien, C. L. Magnetic properties and colossal magnetoresistance of La(Ca)MnO_3 materials doped with Fe. *Phys. Rev. B* **1996**, *54*, 15299−15302.
(86) Boyer, L. L.; Kaxiras, E.; Feldman, J. L.; Broughton, J. Q.; Mehl, M. J. New low-energy crystal structure for silicon. *Phys. Rev. Lett.* **1991**, *67*, 715−718.
(87) Katriel, J. A study of the interpretation of Hund's rule. *Theor. Chim. Acta* **1972**, *23*, 309−315.
(88) Fang, Z.; Zhao, W.; Shen, T.; Qiu, D.; Lv, Y.; Hou, X.; Hou, Y. Spin-Modulated Oxygen Electrocatalysis. *Precis. Chem.* **2023**, *1*, 395−417.
(89) Suntivich, J.; Gasteiger, H. A.; Yabuuchi, N.; Nakanishi, H.; Goodenough, J. B.; Shao-Horn, Y. Design principles for oxygen-reduction activity on perovskite oxide catalysts for fuel cells and metal−air batteries. *Nat. Chem.* **2011**, *3*, 546−550.
(90) Suntivich, J.; May, K. J.; Gasteiger, H. A.; Goodenough, J. B.; Shao-Horn, Y. A Perovskite Oxide Optimized for Oxygen Evolution Catalysis from Molecular Orbital Principles. *Science* **2011**, *334*, 1383−1385.
(91) Wei, C.; Feng, Z.; Scherer, G. G.; Barber, J.; Shao-Horn, Y.; Xu, Z. J. Cations in Octahedral Sites: A Descriptor for Oxygen Electrocatalysis on Transition-Metal Spinels. *Adv. Mater.* **2017**, *29*, No. 1606800.
(92) Gracia, J. Spin dependent interactions catalyse the oxygen electrochemistry. *Phys. Chem. Chem. Phys.* **2017**, *19*, 20451−20456.
(93) Garcés-Pineda, F. A.; Blasco-Ahicart, M.; Nieto-Castro, D.; López, N.; Galán-Mascarós, J. R. Direct magnetic enhancement of electrocatalytic water oxidation in alkaline media. *Nat. Energy* **2019**, *4*, 519−525.
(94) Ge, J.; Ren, X.; Chen, R. R.; Sun, Y.; Wu, T.; Ong, S. J. H.; Xu, Z. J. Multi-Domain versus Single-Domain: A Magnetic Field is Not a Must for Promoting Spin-Polarized Water Oxidation. *Angew. Chem., Int. Ed.* **2023**, *62*, No. e202301721.
(95) Ren, X.; Wu, T.; Gong, Z.; Pan, L.; Meng, J.; Yang, H.; Dagbjartsdottir, F. B.; Fisher, A.; Gao, H. J.; Xu, Z. J. The origin of magnetization-caused increment in water oxidation. *Nat. Commun.* **2023**, *14*, 2482.
(96) Berkowitz, A. E.; Lahut, J. A.; Jacobs, I. S.; Levinson, L. M.; Forester, D. W. Spin Pinning at Ferrite-Organic Interfaces. *Phys. Rev. Lett.* **1975**, *34*, 594−597.
(97) Ong, Q. K.; Wei, A.; Lin, X.-M. Exchange bias in Fe/Fe_3O_4 core-shell magnetic nanoparticles mediated by frozen interfacial spins. *Phys. Rev. B* **2009**, *80*, No. 134418.
(98) Ge, J.; Chen, R. R.; Ren, X.; Liu, J.; Ong, S. J. H.; Xu, Z. J. Ferromagnetic−Antiferromagnetic Coupling Core−Shell Nanoparticles with Spin Conservation for Water Oxidation. *Adv. Mater.* **2021**, *33*, No. 2101091.
(99) Yao, Y.; Hu, S.; Chen, W.; Huang, Z.-Q.; Wei, W.; Yao, T.; Liu, R.; Zang, K.; Wang, X.; Wu, G.; Yuan, W.; Yuan, T.; Zhu, B.; Liu, W.; Li, Z.; He, D.; Xue, Z.; Wang, Y.; Zheng, X.; Dong, J.; Chang, C.-R.; Chen, Y.; Hong, X.; Luo, J.; Wei, S.; Li, W.-X.; Strasser, P.; Wu, Y.; Li, Y. Engineering the electronic structure of single atom Ru sites via compressive strain boosts acidic water oxidation electrocatalysis. *Nat. Catal.* **2019**, *2*, 304−313.
(100) Nong, H. N.; Reier, T.; Oh, H.-S.; Gliech, M.; Paciok, P.; Vu, T. H. T.; Teschner, D.; Heggen, M.; Petkov, V.; Schlögl, R.; Jones, T.; Strasser, P. A unique oxygen ligand environment facilitates water oxidation in hole-doped $IrNiO_x$ core−shell electrocatalysts. *Nat. Catal.* **2018**, *1*, 841−851.
(101) Deng, Y.; Luo, J.; Chi, B.; Tang, H.; Li, J.; Qiao, X.; Shen, Y.; Yang, Y.; Jia, C.; Rao, P.; Liao, S.; Tian, X. Advanced Atomically Dispersed Metal−Nitrogen−Carbon Catalysts Toward Cathodic Oxygen Reduction in PEM Fuel Cells. *Adv. Energy Mater.* **2021**, *11*, No. 2101222.
(102) Li, L.; Zhou, J.; Wang, X.; Gracia, J.; Valvidares, M.; Ke, J.; Fang, M.; Shen, C.; Chen, J.-M.; Chang, Y.-C.; Pao, C.-W.; Hsu, S.-Y.; Lee, J.-F.; Ruotolo, A.; Chin, Y.; Hu, Z.; Huang, X.; Shao, Q. Spin-Polarization Strategy for Enhanced Acidic Oxygen Evolution Activity. *Adv. Mater.* **2023**, *35*, No. 2302966.
(103) Gao, C.; Wang, J.; Hübner, R.; Zhan, J.; Zhao, M.; Li, Y.; Cai, B. Spin Effect to Regulate the Electronic Structure of Ir−Fe Aerogels for Efficient Acidic Water Oxidation. *Small* **2024**, *20*, No. 2400875.

https://doi.org/10.1021/acsmaterialsau.4c00092
ACS Mater. Au 2025, 5, 253−267